© 2017. Published by The Company of Biologists Ltd | Development (2017) 144, 3686-3697 doi:10.1242/dev.155077

STEM CELLS AND REGENERATION

RESEARCH ARTICLE

Zfp423/*ZNF423* regulates cell cycle progression, the mode of cell division and the DNA-damage response in Purkinje neuron progenitors

Filippo Casoni[1,2,§], Laura Croci[1,§], Camilla Bosone[1,2], Roberta D'Ambrosio[1], Aurora Badaloni[1], Davide Gaudesi[1], Valeria Barili[1,2,‡], Justyna R. Sarna[3], Lino Tessarollo[4], Ottavio Cremona[1,2], Richard Hawkes[5], Søren Warming[4,*] and G. Giacomo Consalez[1,2,¶]

ABSTRACT

The *Zfp423*/*ZNF423* gene encodes a 30-zinc-finger transcription factor involved in key developmental pathways. Although null *Zfp423* mutants develop cerebellar malformations, the underlying mechanism remains unknown. *ZNF423* mutations are associated with Joubert Syndrome, a ciliopathy causing cerebellar vermis hypoplasia and ataxia. *ZNF423* participates in the DNA-damage response (DDR), raising questions regarding its role as a regulator of neural progenitor cell cycle progression in cerebellar development. To characterize *in vivo* the function of ZFP423 in neurogenesis, we analyzed allelic murine mutants in which distinct functional domains are deleted. One deletion impairs mitotic spindle orientation, leading to premature cell cycle exit and Purkinje cell (PC) progenitor pool deletion. The other deletion impairs PC differentiation. In both mutants, cell cycle progression is remarkably delayed and DDR markers are upregulated in cerebellar ventricular zone progenitors. Our *in vivo* evidence sheds light on the domain-specific roles played by ZFP423 in different aspects of PC progenitor development, and at the same time strengthens the emerging notion that an impaired DDR may be a key factor in the pathogenesis of JS and other ciliopathies.

KEY WORDS: Joubert syndrome, Cerebellar development, Purkinje cell development, DNA-damage response, Cell cycle progression/exit, Progenitor maintenance

INTRODUCTION

Within the cerebellar primordium, two neurogenic matrices are discernible: the ventricular zone (VZ) and the anterior rhombic lip (RL) (reviewed by Leto et al., 2015). Starting at E10.5-E11.5 (Goldowitz and Hamre, 1998), the cerebellar VZ, which is positive for PTF1A (Hoshino et al., 2005), neurogenin 1 and neurogenin 2 (Salsano et al., 2007; Zordan et al., 2008), ASCL1 (Grimaldi et al., 2009), and the adhesion molecules NEPH3 and E-cadherin (Mizuhara et al., 2009), gives rise in overlapping waves to all γ-aminobutyric acid (GABA)-positive neurons, including PCs (Florio et al., 2012; Kim et al., 2011a; Lundell et al., 2009) and GABAergic interneurons, which are born sequentially from a common $PAX2^+$ progenitor pool (Leto et al., 2006, 2009; Maricich and Herrup, 1999; Weisheit et al., 2006).

Defects affecting the VZ or RL translate into congenital malformations of the cerebellum. Individuals affected by congenital ataxias suffer motor disability, muscular hypotonia and incoordination. Malformations involve the cerebellar vermis, and are sometimes accompanied by other neural and extraneural abnormalities. Joubert syndrome (JS, MIM21330) is a debilitating multisystem ciliopathy displaying a distinctive malformation of the brainstem and cerebellar peduncles called the molar tooth sign for its appearance in axial MRI sections. It is characterized by congenital malformation of the brainstem and agenesis or hypoplasia of the cerebellar vermis, leading to ataxia, breathing dysregulation, nystagmus, hypotonia and a delay in achieving motor milestones, and possibly affecting cognitive function. JS is usually inherited as an autosomal recessive trait and is caused by mutations in genes encoding proteins that localize either in the primary cell cilium or centrosome/basal body/transition zone (reviewed by Romani et al., 2013). These proteins control ciliary structure/stability, and signal transduction (reviewed by Goetz and Anderson, 2010; Han and Alvarez-Buylla, 2010).

Zfp423-deficient mice display a variety of developmental defects, including a completely penetrant cerebellar vermis hypoplasia (CVH) (Alcaraz et al., 2006; Cheng et al., 2007; Warming et al., 2006). Malformations of cerebellar hemispheres are dependent on modifier genes and stochastic factors (Alcaraz et al., 2011). Importantly, individuals carrying *ZNF423* gene mutations/deletions have been diagnosed with JS, CVH, nephronophthisis (NPHP) and other signs of ciliopathy (Chaki et al., 2012). Although ZFP423 has been convincingly implicated in the cilium-mediated response to sonic hedgehog (SHH) during cerebellar granule cell (GC) proliferation (Hong and Hamilton, 2016), our observations clearly point to an additional key role for this protein in PC development long before the onset of GC clonal expansion. Incidentally, GC clonal expansion relies on SHH released by PCs starting before birth (Dahmane and Ruiz-i-Altaba, 1999; Wallace, 1999; Wechsler-Reya and Scott, 1999), so that the final number of GCs is heavily influenced by the total number of postmitotic PCs.

Zfp423 encodes a 30 zinc-finger nuclear protein that works both as a scaffold and as a transcription factor, cooperating with multiple regulatory molecules. Through a domain spanning zinc fingers 9-20, ZFP423 acts a co-activator in BMP (Hata et al., 2000) and Notch (Masserdotti et al., 2010) signaling pathways. Although the

[1]Division of Neuroscience, San Raffaele Scientific Institute, Milan 20132, Italy. [2]Università Vita-Salute San Raffaele, Milan 20132, Italy. [3]Department of Clinical Neurosciences and Hotchkiss Brain Institute, Cumming School of Medicine, University of Calgary, Alberta AB T2N 1N4, Canada. [4]Center for Cancer Research, National Cancer Institute, Frederick, MD 21702-1201, USA. [5]Department of Cell Biology & Anatomy and Hotchkiss Brain Institute, Cumming School of Medicine, University of Calgary, Alberta AB T2N 1N4, Canada.
[§]These authors contributed equally to this work
*Present address: Genentech, South San Francisco, CA 94080, USA.
‡Present address: University of Parma, Parma 43121, Italy.

¶Author for correspondence (g.consalez@hsr.it)

F.C., 0000-0002-1172-8377; V.B., 0000-0001-7711-2156; O.C., 0000-0001-9462-1040; G.G.C., 0000-0003-4594-6273

Received 18 May 2017; Accepted 1 September 2017

Development (2017) 144, 3686-3697 doi:10.1242/dev.155077

role of BMP signaling in granule cell development has been clearly established (reviewed by Roussel and Hatten, 2011), its involvement in PC development can only be partially inferred from the analysis of conditional SMAD4-null mice, although SMAD4 is not exclusively a BMP signaling transducer (Massagué, 2000). These mice display a marked decrease in the number of PCs and parvalbumin-positive interneurons (Zhou et al., 2003). As regards Notch, its importance in the genesis of PCs has been characterized through both constitutive (Lütolf et al., 2002) and conditional *Notch1* mutants (Machold et al., 2007) that exhibit a massive decrease in PC number. Moreover, through a C-terminal domain spanning zinc fingers 28-30, ZFP423 interacts with EBF transcription factors (Tsai and Reed, 1997, 1998), which are involved in cerebellar development (Croci et al., 2006, 2011) and molecular patterning of the cerebellar cortex (Chung et al., 2008, 2009). To date, the *Ebf2* null mutation is the only genetic manipulation thus far shown to subvert PC subtype specification (Croci et al., 2006). *Ebf2* acts to repress the zebrin II^{+} phenotype in late-born PCs (Chung et al., 2008). Thus, the possible interaction of ZFP423 with these regulatory signals in the context of PC development remains a relevant unanswered question.

Importantly, ZFP423/ZNF423 also interacts with Poly ADP-ribose polymerase 1 (PARP1) through zinc fingers 9-20 (Ku et al., 2006) and with centrosomal protein 290 (CEP290) through an N-terminal domain (Chaki et al., 2012). PARP1 is a double-stranded (ds) DNA-damage sensor that recruits MRE11 and ataxia-telangectasia mutated (ATM) to sites of DNA damage. CEP290 is a centrosomal protein mutated in JS and NPHP, the loss of which causes enhanced DNA-damage signaling, DNA breaks, replication stress and supernumerary centrioles (Slaats et al., 2015). Because a successful DNA-damage response (DDR) requires a tight control over cell cycle checkpoints, we postulated that defective DNA-damage signaling might delay cell cycle progression, contributing to the hypoplastic cerebellum seen in mutant mice and patients alike. Interestingly, recent evidence supports the notion of a broad role for ciliopathy genes in the DDR: in fact, both CEP290 and NEK8 mutations lead to an accumulation of DNA damage due to disturbed replication forks (Choi et al., 2013; Slaats et al., 2015). Furthermore, increased DNA-damage signaling has been detected in CEP164-, ZNF423- and SDCCAG8-associated renal cells (Airik et al., 2014; Chaki et al., 2012). In the present paper, we describe the results of a detailed *in vivo* analysis of two allelic *Zfp423* in-frame deletion mouse lines, each characterized by nullisomy for a distinct functionally characterized protein-protein interaction domain.

RESULTS

The ZFP423 protein is expressed throughout the VZ, peaking in M-phase ventricular zone progenitors

The distribution of the *Zfp423* transcript in the embryonic CNS has been described previously (Alcaraz et al., 2006; Cheng et al., 2007; Masserdotti et al., 2010; Warming et al., 2006). Here, we report the tissue and subcellular distribution of the corresponding protein in the early cerebellar primordium. On embryonic day 11.5 (E11.5), ZFP423 is abundantly expressed throughout the cerebellar primordium, especially flanking the midline. The protein is found in the rhombic lip (RL), in the roof plate (RP) (arrowheads in Fig. 1A) and in the prospective sub-arachnoid space (SA) (Fig. 1A). Both the RP and the SA space harbor signaling cells important for cerebellar development (*inter alia*, see Aldinger et al., 2009; Chizhikov et al., 2006). In the cerebellar VZ, which contains PC precursors, progenitor cell bodies known as radial glia (Anthony et al., 2004) are arranged into a pseudostratified epithelium and oscillate back and forth from the basal membrane to the apical margin (Florio et al., 2012), which contains an adherens junction belt (Kosodo et al., 2004). This process has been dubbed interkinetic nuclear migration (reviewed by Götz and Huttner, 2005). The location of cell bodies correlates with specific phases of the cell cycle. At the apical most end of their range, bordering the ventricular lumen, progenitors enter M-phase and divide. In the cerebellar VZ, ZFP423 is expressed at its highest levels in M-phase precursors decorated by phosphorylated histone H3 (PHH3) (arrows in Fig. 1B). In the E12.5 VZ, robust ZFP423 expression levels are maintained in M-phase progenitors, and slightly lower levels are found in interphase nuclei scattered throughout the thickness of the VZ (Fig. 1C,C′). A subset of ZFP423 PC progenitors also expresses the marker OLIG2, which is mostly associated with G0/G1 PC progenitors (Ju et al., 2016). Likewise, the domain containing differentiating PC precursors positive for CORL2 colocalizes

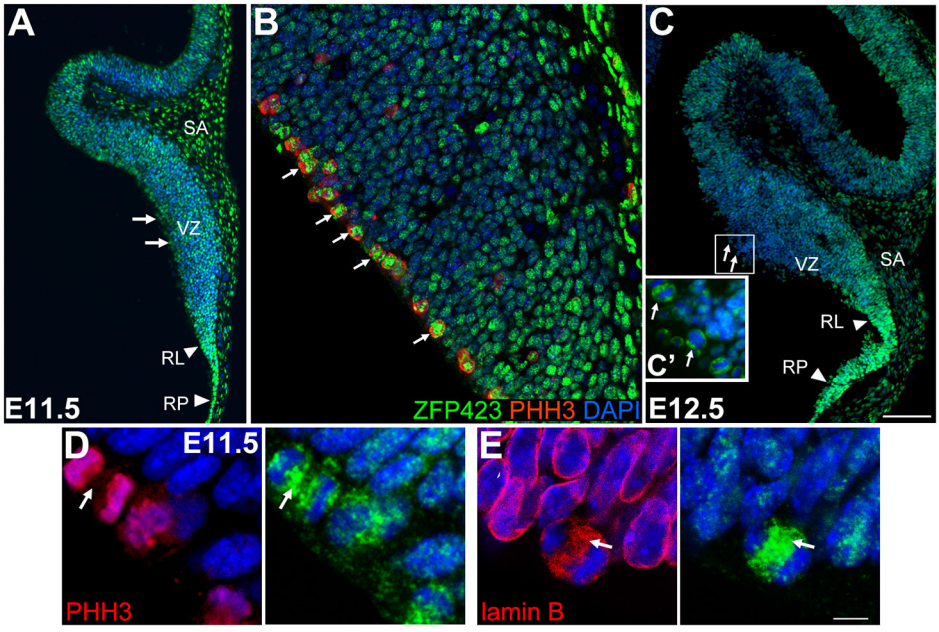

Fig. 1. ZFP423 is expressed in both germinal layers of the cerebellar primordium. Immunofluorescence staining of cerebellar sagittal sections at E11.5 (A,B,D,E) and E12.5 (C). ZFP423 protein levels in medial sections (e.g. A) are higher than in lateral sections (e.g. B). (A-C) The ZFP423 protein is expressed in the cerebellar primordium, including the ventricular zone (arrows), the germinal layer that produces all GABAergic neurons and PCs in particular. (B) ZFP423 is strongly expressed in radial glial progenitors positive for the M-phase marker PHH3 (arrows in B). (D,E) Whereas in interphase cells ZFP423 is mostly detected in the nucleus, in dividing PHH3^{+} progenitors the protein is mostly separate from chromatin (arrows in D). In some presumptive anaphase cells, ZFP423 colocalizes with the nuclear lamina protein lamin B (arrows in E). RL, rhombic lip; RP, roof plate; SA, subarachnoid space; VZ, ventricular zone. Scale bars: 100 µm in A,C; 50 µm in B; 5 µm in D,E.

Development (2017) 144, 3686-3697 doi:10.1242/dev.155077

partially with the ZFP423^{+} postmitotic domain in the cerebellar primordium (Fig. S1). These findings indicate that ZFP423 is expressed in PC progenitors.

At the subcellular level, most of the ZFP423 signal is uncoupled from PHH3^{+} chromatin (Fig. 1D) and overlaps partially with the nuclear intermediate filament lamin B (Fig. 1E). However, we have no conclusive *in vivo* evidence of ZFP423 colocalization with the centrosomal marker γ-tubulin (described by Chaki et al., 2012).

Generation and analysis of two allelic mutants harboring specific ZFP423 domain deletions

To dissect the domain-specific roles of ZFP423 in the events that lead up to PC neurogenesis, we produced two lines of mice by BAC recombineering in *E. coli* and gene targeting in ES cells. Each line carries a distinct targeted deletion of *Zfp423* (sketched in Fig. 2A). The first deletion, dubbed Δ9-20, spans nucleotides 1258-2517 of the ORF (420 amino acids), encoding zinc fingers 9-20. The corresponding protein domain mediates a molecular interaction with the BMP-responsive element (BRE) and SMAD1-SMAD4 (Hata et al., 2000), and with PARP1 (Chaki et al., 2012; Ku et al., 2003). Moreover, this domain is required for the functional interaction with the Notch intracellular domain (Masserdotti et al., 2010). The second deletion, called Δ28-30, removes nucleotides 3861-4108 of the ORF and causes a frameshift mutation that produces a stop codon 158 bp into exon 8. The resulting C-terminally truncated protein lacks zinc fingers 28-30 and 91 C-terminal amino acids. This domain has been implicated in the interaction with the Collier/Olf-1/EBF (COE) family of transcription factors (Tsai and Reed, 1997). Heterozygous mutants of both genotypes are viable and fertile, and display no overt phenotypic abnormality, suggesting that neither mutation has any relevant toxic gain-of-function or dominant-negative effect (not shown). Conversely, homozygous mutants, on a C57BL/6N background, have a highly significant increase in lethality compared with wild-type littermates by postnatal day 7 (χ^2 test, P<0.0001). Survivors (~3%) are profoundly ataxic, replicating findings described in null mutants. Histological analysis of prenatal mouse cerebella (E18.5, Fig. S2) and the whole-mount analysis of young adult cerebella from outbred [(C57BL/6Nx129S1/SVImJ) F2] mutants revealed that homozygotes for both mutations exhibit severe cerebellar hypoplasia, with a markedly reduced vermis. The Δ28-30 mutant features a pronounced posterior vermis deletion that is more evident than in the Δ9-20 (Fig. 2B). The corresponding mutant genes are upregulated with respect to the wild type (Fig. 2C), as expected based on published results (Cho et al., 2013). Both deleted proteins (sketched in Fig. S3) retain the DNA-binding domain spanning zinc fingers 2-8 (Tsai and Reed, 1998) and are stable, as shown by a western blot of embryonic cerebellar lysates (Fig. 2D). Deletion products retain a nuclear localization in E12.5 cerebellar primordia (Fig. 2E). Protein stability and antibody

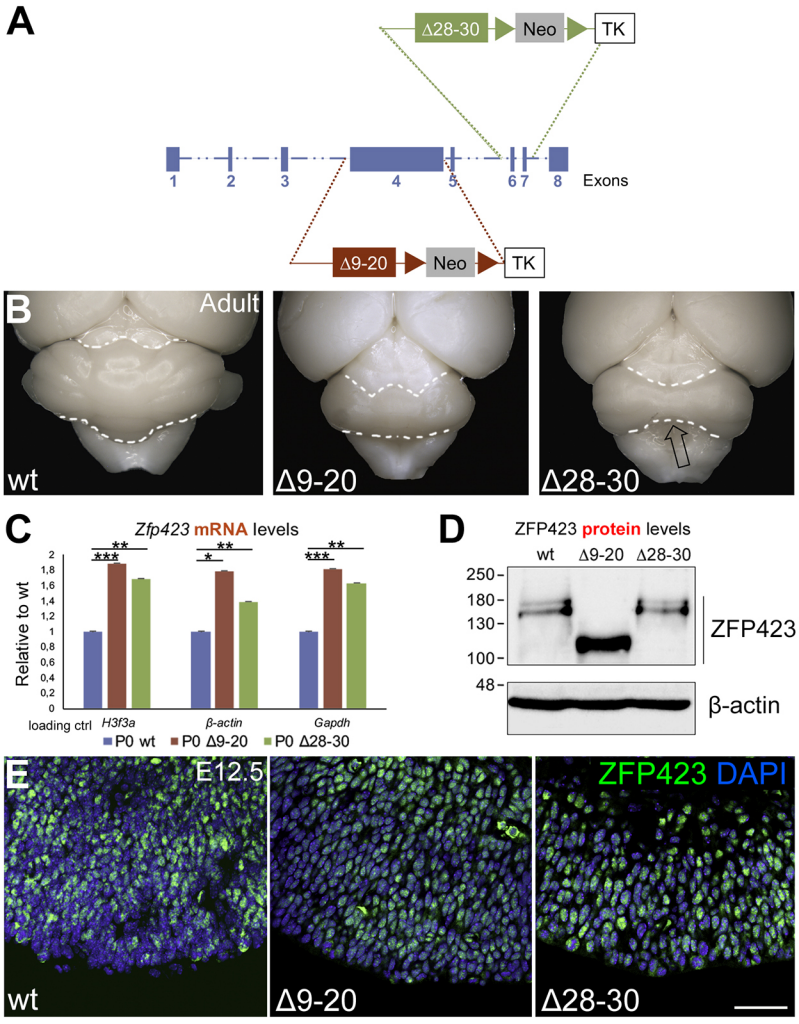

Fig. 2. Both *Zfp423* deletion mutants produce a stable predominantly nuclear protein and exhibit a severe cerebellar hypoplasia. (A) Schematic representation of the constructs produced to generate, by homologous recombination, the Δ9-20 and Δ28-30 allelic mutants. (B) Dorsal view of cerebellar malformations in adult mutant mice, compared with the control. In homozygosity, both mutants display a decreased cerebellar size and a severe vermis hypoplasia, with a more pronounced posterior deletion in the Δ28-30 (arrow in B). (C,D) At P0, both deleted RNAs (RT-qPCR in C) and proteins (western blot in D) are expressed at robust levels and proteins migrate near expected sizes. Mutant transcripts are significantly upregulated compared with the wild type (n=3; data are mean±s.d.; Welch's t-test: *P<0.05; **P<0.01; ***P<0.005). (E) ZFP423 immunostaining of E12.5 sagittal cerebellar sections reveals that, *in vivo*, both deleted proteins are expressed and localize predominantly in the cell nucleus. Scale bar: 25 µm in E.

Development (2017) 144, 3686-3697 doi:10.1242/dev.155077

specificity were confirmed through immunofluorescence in murine kidney IMCD-3 cells, which do not express endogenous ZFP423, transfected with myc-tagged ZFP423 constructs, wild-type and both deletion products.

The number of PCs is decreased in both allelic *Zfp423* mutants

Zfp423-null mutant embryos showed reduced BrdU incorporation in the cerebellar VZ at E14.5 (Alcaraz et al., 2006); however, at that stage, PC progenitors no longer proliferate. We conducted PC counts after the end of PC progenitor proliferation (E18.5, P17). These indicated a substantial drop in the number of PCs in both mutants. In particular, at P17, the perimeter of the PC layer in both mutants ranges between 27% and 60% of normal, depending on distance from the midline, with the sharpest decrease in the cerebellar vermis (Fig. 3A), whereas the numerical density of calbindin^{+} cell bodies is normal in the mutant PC layer. These results demonstrate that *Zfp423* mutation causes a severe drop in PC number. In keeping with this evidence, the total PC number, as measured by counting immature CORL2^{+} PCs in the fetal cerebellar cortex (E18.5), is sharply reduced in both allelic mutant cerebella (Fig. 3B). Based on this evidence, we asked whether the PC loss scored in our allelic mutants affects both zebrinII^{+} and zebrinII^{-} PC subtypes or is selective for a specific subpopulation. In the adult cerebellum, PCs are arranged in two (mostly) mutually exclusive parasagittal patterns – one characterized by zebrin II/aldolase C expression (Brochu et al., 1990), the other by the expression of PLCβ4 (Sarna et al., 2006). These subsets correspond to early-born and late-born PC populations, respectively (Croci et al., 2006; Hashimoto and Mikoshiba, 2003; Larouche and Hawkes, 2006). Our results (Fig. 3C) show that the Δ28-30 cerebellum, albeit smaller, contains a balanced complement of both PC types, whereas the Δ9-20 shows a selective loss of late-born (PLCβ4^{+}) progenitors (see full characterization in Fig. S5). Taken together, our findings suggest that both *Zfp423* mutants display a severe loss of PCs, and that in the Δ9-20 cerebellar primordium, PC progenitors may leave the cell cycle and differentiate prematurely, depleting the progenitor pool. This is in contrast to Δ28-30, where early- and late-born PCs are present in approximately normal proportions.

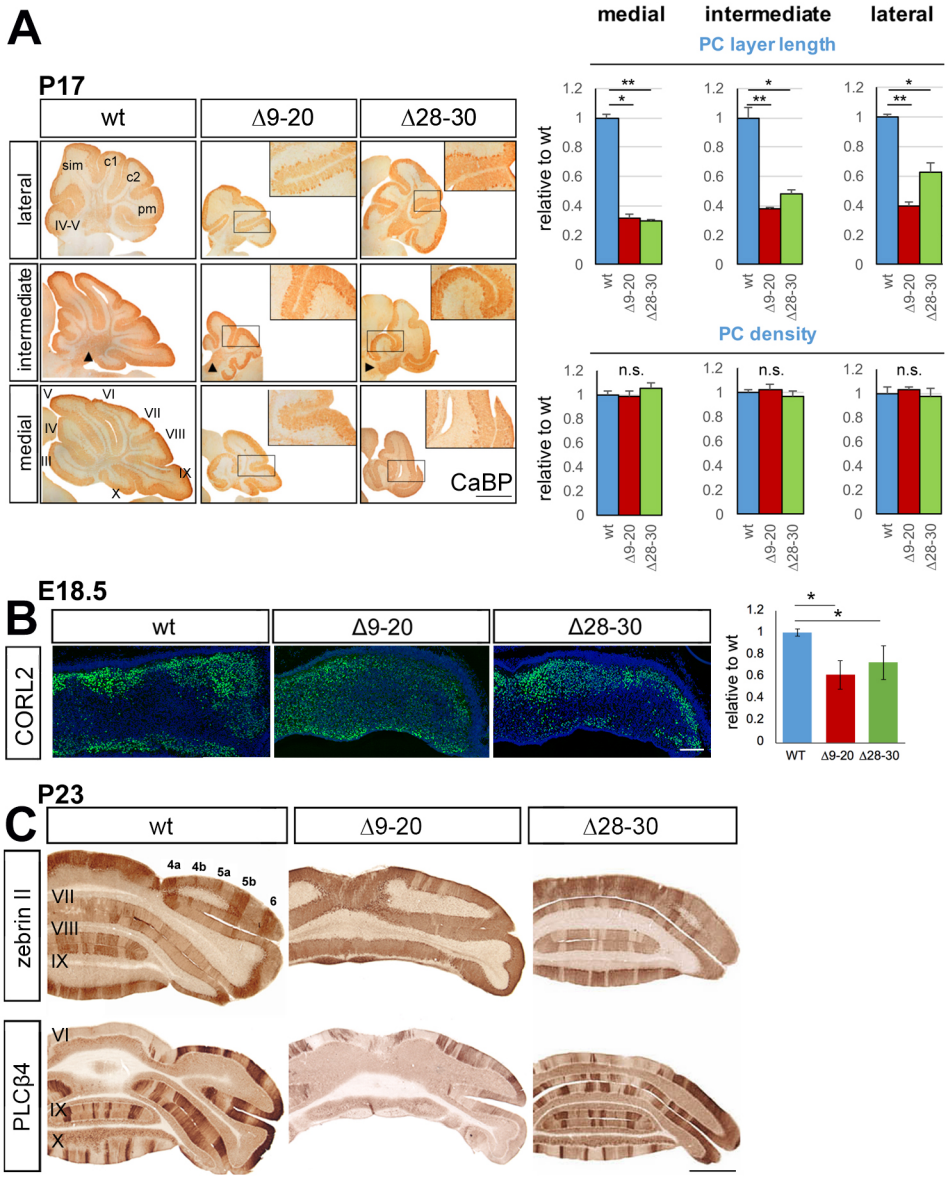

Fig. 3. Although PC numbers are reduced in both mutants, the Δ9-20 selectively lacks late-born Purkinje cells. (A) Left: immunohistochemistry of P17 sagittal sections stained for the PC-specific marker calbindin (CaBP). Cerebellar hypoplasia is evident in both mutants. Right: morphometric analysis results point to a severe decrease in the PC layer perimeter in both mutants, more pronounced in the cerebellar vermis than the hemispheres; on the contrary, PC numerical density is unchanged. This analysis was conducted using ImageJ (NIH) software and results are plotted as the mean±s.e.m. n=3/genotype; *P<0.01; **P<0.005, Welch's t-test. (B) Corl2 immunofluorescence staining (green) of E18.5 frontal sections reveals a severe PC loss in both mutant cerebella compared with wild-type controls using three different loading controls. The total Corl2^{+} PCs were counted using ImageJ (NIH) software, and the result is plotted as the mean±s.e.m. (n=3 for each genotype; *P<0.05; Welch's t-test). (C) The results of zebrin II and PLCβ4 immunostaining of P23 frontal cerebellar sections reveal a selective depletion of late-born PCs (PLCβ4+) in Δ9-20 mutants. Conversely, the Δ28-30 mutant cerebellum, albeit smaller, contains a balanced representation of early- (zebrin II^{+}) and late-born (PLCβ4^{+}) PCs. Sim, simplex; c1, crus1; c2, crus2; pm, paramedian. Scale bars: 200 µm in B; 1 mm in A,C.

Development (2017) 144, 3686-3697 doi:10.1242/dev.155077

Allelic *Zfp423* deletions have divergent effects on PC progenitor maintenance and differentiation

To try to clarify the events leading to PC depletion in *Zfp423* mutants, immunofluorescence was used to analyze markers of mitotic (OLIG2+) and postmitotic (CORL2+, LHX5+) PC precursors at E12.5, when PC neurogenesis peaks (Minaki et al., 2008; Seto et al., 2014; Wang et al., 2011; Zhao et al., 2007). Our results indicate that, at E12.5, the domain containing mitotic and postmitotic OLIG2$^+$ PC progenitors (Seto et al., 2014) (Fig. 4A) is significantly reduced in the Δ9-20 cerebellar primordium, while it is expanded in the Δ28-30 primordium. Because the VZ gives rise to cell types other than PCs, including GABAergic interneurons and astroglia (reviewed by Leto et al., 2015), we analyzed markers of both populations. At E12.5, both proliferating GABA interneuron progenitors (*Gsx1*+) and PAX2$^+$ postmitotic precursors are depleted in the Δ9-20 cerebellum (Fig. S6A,B, respectively). Regarding SOX9 astroglial progenitors, they are depleted at E14.5 in both mutants, more so in the Δ9-20 (Fig. S6C,C′).

Next, we investigated the role of ZFP423 in the context of PC differentiation. The expression level of CORL2, a PC progenitor differentiation marker, is reduced in the Δ9-20 (Fig. 4B,B′), reflecting the observed decline in the number of OLIG2$^+$ mitotic cells (Fig. 4A, A′). At the same stage, CORL2 levels (Fig. 4B,B′) are decreased in the Δ28-30 cerebellum, despite the abundance of OLIG2$^+$ cells; this suggests a severe defect/delay in PC progenitor differentiation, such that the CORL2/OLIG2 ratio (Fig. 4B″) is profoundly decreased in this mutant. The *Lhx5* transcript distribution, analyzed by *in situ* hybridization (Fig. 4C), parallels and supports the described CORL2 results. To investigate cell death as a possible reason for the decrease in VZ progenitors observed in the Δ28-30, we performed TUNEL staining on E14.5 sagittal sections; however, this failed to detect any significant cell death in the VZ of either mutant (Fig. 4D). The two allelic mutations therefore have different effects on the ratio of differentiating to proliferating progenitors.

Mutations affecting mitotic spindle stability switch the mode of cell division from equal/proliferative to unequal/neurogenic (Fish et al., 2006), arresting the expansion of the stem cell pool. It is well established that the transition from proliferative to neurogenic cell division of apical radial glial progenitors correlates with a change in the M-phase cleavage plane from vertical to oblique/horizontal (Gertz et al., 2014), and with an unequal inheritance of the apical adherens junction (the ‘cadherin hole’) in the two daughter cells (Kosodo et al., 2004). Through its dynamic interaction with the centrosomal protein CEP290 (Chaki et al., 2012), itself a Joubert syndrome gene, or via its role as a transcriptional regulator, ZFP423 may affect the stability/orientation of the mitotic spindle. To evaluate the effect of *Zfp423* mutations on spindle orientation and the type of cell division, we analyzed anaphase figures in the E11.5 cerebellar VZ, in both mutants and controls (representative images are in Fig. 5A). Our assessment of equal (arrows) versus unequal cell divisions (arrowhead) (both PHH3 positive) was based on (1) the orientation of the cell division plane with respect to the ventricular surface (Gertz et al., 2014); and (2) the equal or unequal inheritance of the cadherin hole (Kosodo et al., 2004) (see Materials and Methods). Our results, obtained by analyzing at least three independent embryos per genotype, are shown in Fig. 5B and indicate that, in the Δ9-20 cerebellar VZ (n=60 mitoses tested), the number of unequal cell divisions is significantly increased compared with the wild type (n=99) (**P<0.01, Fisher’s exact test), consistent with a shift from proliferative to neurogenic cell divisions in this mutant. Conversely, Δ28-30 mitoses (n=89) show a trend towards an excess of equal cell cleavages compared with the

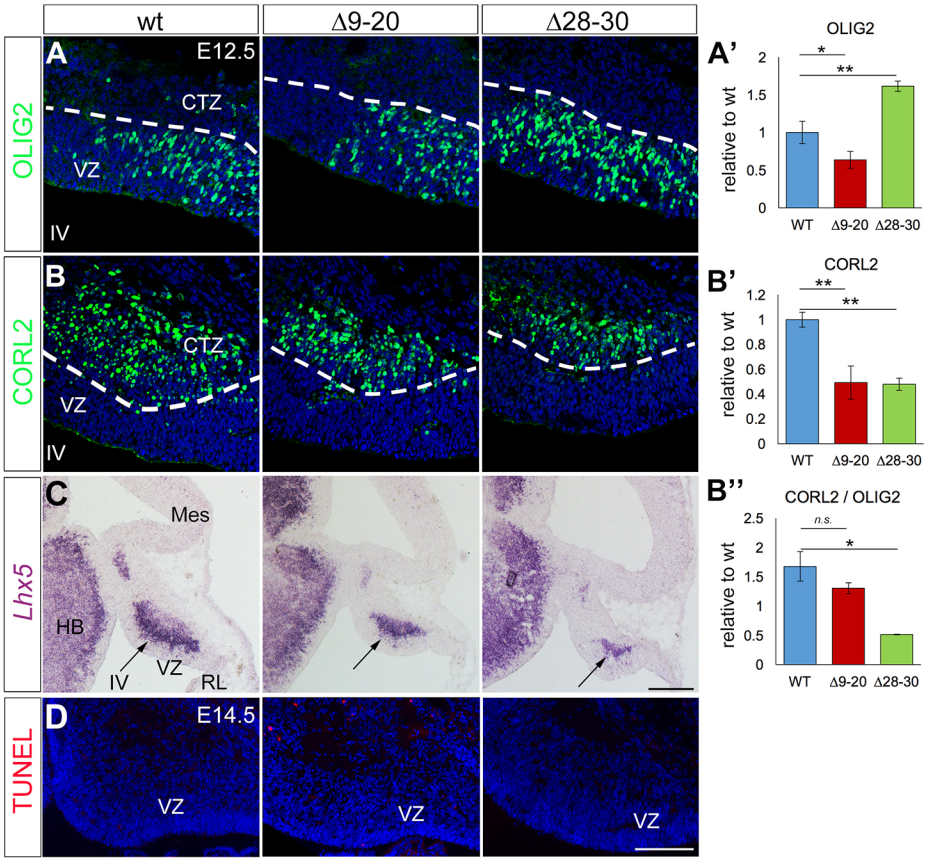

Fig. 4. In the cerebellar primordium, ZFP423 controls the proliferation and differentiation of PC progenitors. Immunofluorescence staining (A,B) and *in situ* hybridization (C) of cerebellar sagittal sections at E12.5 (rostral to the left). (A) The number of OLIG2$^+$ proliferating PC progenitors is decreased in the Δ9-20 and increased in the Δ28-30, with respect to the wild-type control (quantification in A′; n=3/genotype, *P<0.05; **P<0.01, Welch’s t-test). (B) CORL2$^+$ postmitotic PC precursors are strongly reduced in both mutants (quantification in the B′; n=3/genotype, **P<0.01, Student’s t-test), whereas the CORL2/OLIG2 ratio (B″) is significantly altered only in the Δ28-30 mutants (quantification in the graph; *P<0.05, Welch’s t-test). (C) *Lhx5* (arrows), another marker of early PC differentiation, is downregulated in both mutants compared with wild-type controls. (D) TUNEL staining detected no relevant occurrence of cell death in the mutant or wild-type ventricular zone at E14.5. All results are plotted as mean±s.e.m. of biological triplicates. CTZ, cortical transitory zone; VZ, ventricular zone; IV, fourth ventricle; Mes, mesencephalon; HB, hindbrain; RL, rhombic lip. Scale bars: 40 µm in A,B; 200 µm in C; 60 µm in D.

Development (2017) 144, 3686-3697 doi:10.1242/dev.155077

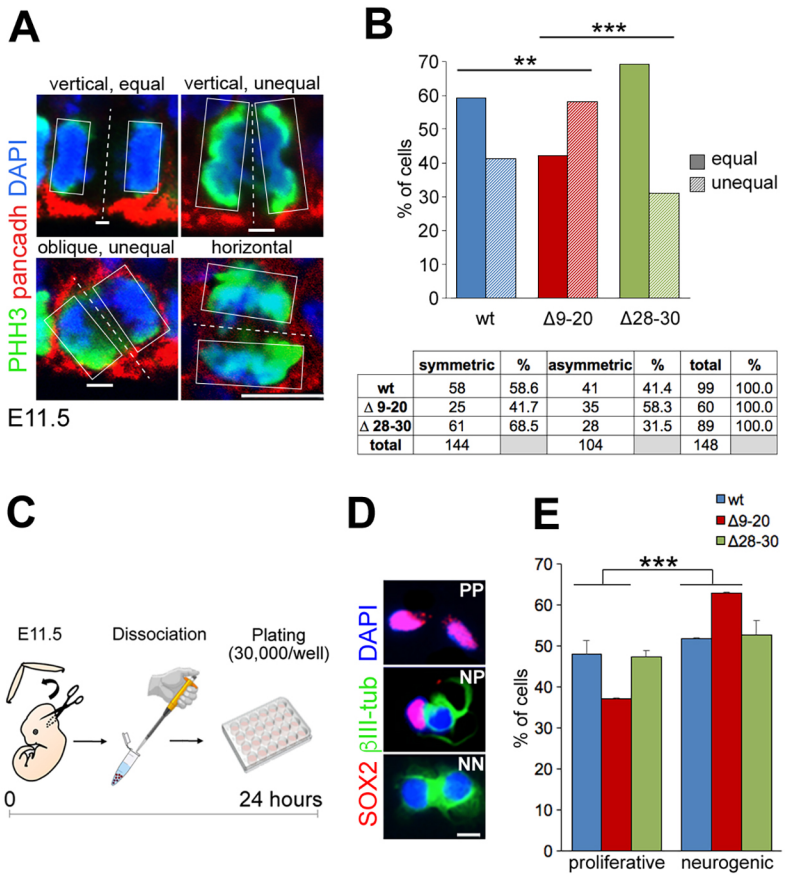

	symmetric	%	asymmetric	%	total	%
wt	58	58.6	41	41.4	99	100.0
Δ 9-20	25	41.7	35	58.3	60	100.0
Δ 28-30	61	68.5	28	31.5	89	100.0
total	144		104		148	

Fig. 5. The Δ9-20 deletion causes a premature switch from proliferative to neurogenic progenitor divisions in the cerebellar VZ. (A) Immunofluorescence staining of the E11.5 cerebellar VZ shows the distribution of PHH3, an M-phase marker, and pancadherin (pancadh), decorating the apical adhesion complex in four sample mitoses. Mitoses were classified taking account of both the angle of the cleavage plane (dashed line) with respect to the ventricular surface and the position of the cadherin hole (solid white line), as described in the Materials and Methods. (B) Quantification of equal and unequal cell divisions in Δ9-20 and Δ28-30 mutants versus controls. *n*=3/genotype, $^{**}P<0.01$; $^{***}P<0.0001$, Fisher's exact test. (C) Flowchart of the cell pair assay protocol (see Materials and Methods). (D) Sample outcomes of symmetric (PP panel and NN panels, respectively) and asymmetric (NP panel) cell divisions in the cerebellar VZ. $Sox2^+/Sox2^+$, proliferative division; $\beta III\text{-}Tub^+/\beta III\text{-}Tub^+$, self-consuming neurogenic division; $Sox2^+/\beta III\text{-}Tub^+$, asymmetric neurogenic division. (E) Quantification of the percentages of proliferative and neurogenic daughter-cell pairs divisions. The results are plotted as the mean±s.d. *n*=3/genotype; $^{***}P<0.0001$, Fisher's exact test. Scale bars: 10 µm in A (bottom right); 5 µm in D.

wild-type VZ that falls just short of statistical significance (P=0.056, Fisher's exact test). A comparison of equal-to-unequal ratios in Δ9-20 versus. Δ28-30 reveals a strongly significant difference ($^{***}P<0.0001$, Fisher's exact test).

To determine whether the observed changes in spindle orientation correlate with an overall switch from proliferative to neurogenic cell division, we conducted a clonal cell-pair assay (procedure sketched in Fig. 5C) (Bultje et al., 2009; Li et al., 2003) on primary cultures of cerebellar VZ progenitors. Admittedly, this *in vitro* assay yields an underestimate of the number of asymmetric cell divisions compared with the *in vivo* situation (Bultje et al., 2009). Embryonic day 11.5 cerebellar primordia were dissociated and neural progenitor cells (NPCs) plated at clonal dilutions. Cells were fixed 24 h later and immunostained for SOX2 (undifferentiated progenitors, P) and neural-specific β-tubulin III (differentiating neurons, N). Daughter cell pairs were subdivided in two categories: PP and NP+NN (sample mitoses in Fig. 5D). Our results (Fig. 5E) indicate that Δ9-20 NPCs (*n*=852) display a cumulative increase in the ratio of neurogenic (NP+NN) to proliferative (PP) divisions, compared with wild type and Δ28-30 (*n*=1339 and 1021, respectively) ($^{***}P<0.0001$, Fisher's exact test).

Thus, both *in vivo* and *in vitro* data (with the caveat that the latter represents a first approximation of the *in vivo* setting, and may lack the contribution of non-cell-autonomous factors) point to a role for the domain that spans zinc fingers 9-20 in maintaining a pool of undifferentiated progenitors in the cerebellar VZ.

The DDR is impaired in *Zfp423* mutant cerebellar VZ progenitors

In an attempt to explain the overall decrease in PC numbers observed in both mutants, we analyzed cell cycle progression of VZ progenitors at E12.5 in three embryos per genotype, belonging to independent litters. In particular, we examined the transition between S and M phase, which encompasses the G_2-M cell cycle checkpoint. To this end, pregnant dams were given a single EdU pulse 30 min prior to sacrifice. Embryonic day 12.5 cerebellar sections were stained for EdU and the M-phase marker PHH3. Our results (Fig. 6A) indicate that, although the number of S-phase progenitors is not diminished in our mutants, both exhibit a significant increase (about 40%) in the ratio of S- to M-phase progenitors, suggesting that cell cycle progression is arrested, at least in some cells, during this transition ($^*P<0.01$ and $^{**}P<0.001$, respectively; Fisher's exact test). When we pulsed pregnant dams 3 h before sacrifice, in the mutant progeny, all M-phase cells ($PHH3^+$) had incorporated EdU (Fig. S7). Considering that at E12.5 (G_2+M) duration equals 2 h (Florio et al., 2012), our evidence, taken together, suggests that in *Zfp423* mutants some cells progress through the S-M phase at a normal pace, while other cells are stalled. To further confirm this observation, we stained sections for PHH3 and looked at the ratio of dotted $PHH3^+$ (G_2) to solid $PHH3^+$ (M phase) signal (Van Hooser et al., 1998). Again, our results clearly indicate that both the Δ9-20 and Δ28-30 cerebellar primordia exhibit an increased ratio of G_2 to M progenitors ($^*P<0.01$ and $^{**}P<0.001$, respectively; Fisher's exact test) (Fig. 6B).

ZNF423 has been linked to the DDR (Chaki et al., 2012). DNA-damage repair is tightly connected to the regulation of cell cycle progression (reviewed by Branzei and Foiani, 2008). Single-strand gaps or nicks and double-strand breaks (DSBs) often occur during S phase and trigger repair by non-homologous end joining (NHEJ) and/or homologous recombination (HR) in mitotic cells. In normal neural tube development, the rapid pace of cell division set by neural progenitors likely exposes them to a high degree of

Development (2017) 144, 3686-3697 doi:10.1242/dev.155077

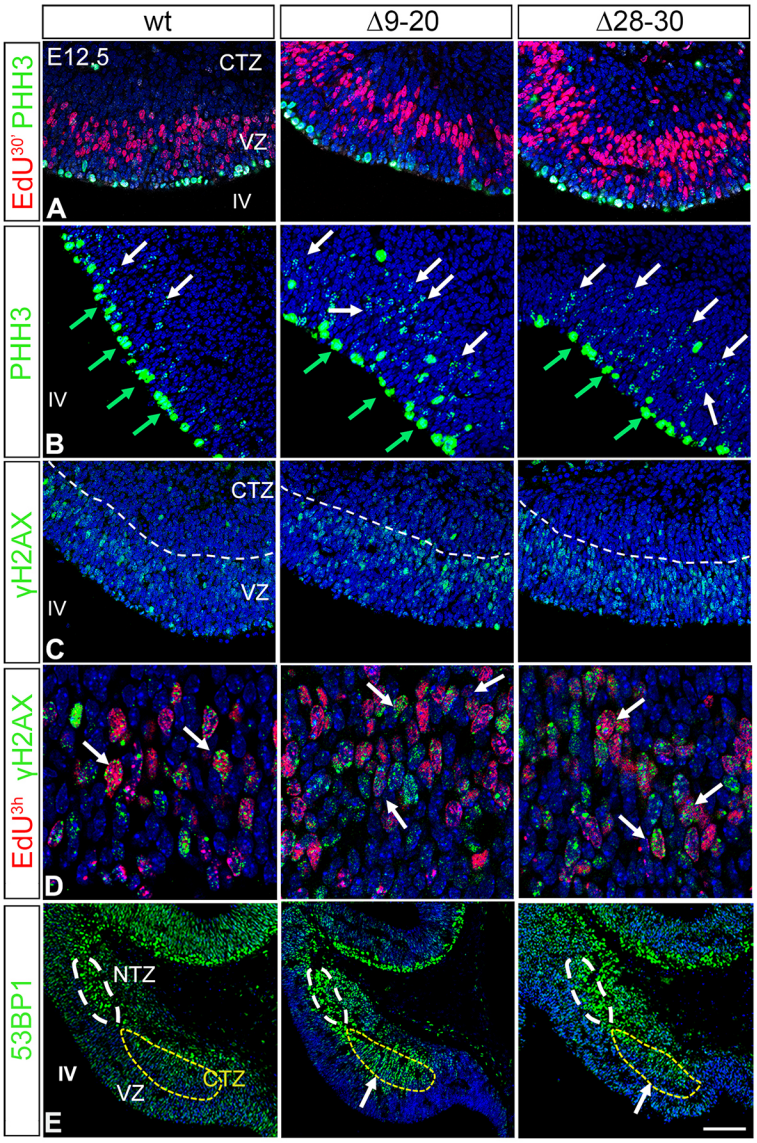

Fig. 6. Stall of cell cycle progression and increase in DNA-damage signaling in the VZ of ZFP423 mutants. (A-E) Sagittal sections of the cerebellar primordium at E12.5 stained for markers of specific cell cycle stages and DNA-damage signaling (rostral towards the left). (A) PHH3 and EdU (single 30′ pulse) label M- and S-phase progenitors, respectively. The graph on the right shows that the ratio between S and M phases is increased in the mutants (n=3/genotype; *P<0.01 and **P<0.001, Fisher's exact test). (B) Dotted (white arrows) and full (green arrows) PHH3 label G_2 and M-phase progenitors, respectively. The graph on the right shows that the ratio between G_2 and M phases is increased in the mutants (n=3/genotype; *P<0.01 and **P<0.001, Fisher's exact test). (C) The density of γH2AX staining, a marker of double-strand breaks, is significantly increased in the cerebellar VZ of both mutants (n=3/genotype; ***P<0.0001, one-way ANOVA, Kruskal–Wallis test, Dunn's multiple comparison test). Dashed line indicates the border between ventricular zone (VZ) and subventricular cortical transitory zone (CTZ), containing mitotic and postmitotic PC progenitors, respectively. (D) Colocalization of γH2AX with EdU (red), shown by arrows, after a 3 h single pulse is strongly upregulated in both mutants (n=3/genotype; *P<0.02; ***P<0.0001, one-way ANOVA, Kruskal–Wallis test, Dunn's multiple comparison test). (E) In both mutants, 53BP1 expression (green) is significantly upregulated in the cortical transitory zone (arrows) (domain c2; Chizhikov et al., 2006) and downregulated in the VZ (arrowheads). Scale bar: 40 µm in A-C; 15 µm in D; 60 µm in E. All results are plotted as mean±s.e.m. IV, fourth ventricle; VZ, ventricular zone; CTZ, cortical transitory zone; NTZ, nuclear transitory zone.

endogenous DNA damage (stalled replication forks leading to single- and double-strand breaks), requiring repair prior to cell division (reviewed by McKinnon, 2013). The finding of mutant progenitors stalled during their G2-M phase transition prompted us to ask whether DNA-damage signaling is increased *in vivo* in *Zfp423* mutants. To test this hypothesis, we immunostained E12.5 cerebellar sections for the DNA-damage marker phosphorylated histone 2A family member X (γH2AX) (Celeste et al., 2002). Our results (Fig. 6C) point to a sharp increase in DNA-damage signaling in the cerebellar VZ of both mutants (***P<0.0001, Kruskal–Wallis test). By immunofluorescence, we assessed the percentage of colocalization between EdU^{3h+} cells (S-M) and γH2AX, and observed a significant increase in colocalization in both mutants (*P<0.02; ***P<0.0001, Kruskal–Wallis test). Finally (Fig. 6E), we observed a qualitative and sharp increase in the expression of 53BP1, a protein involved in NHEJ in response to DSBs (reviewed by Panier and Boulton, 2014), in postmitotic precursors (Fig. 6E), indicating that mitotic progenitors carry over DNA damage upon cell cycle exit, likely due to a reduced efficiency of the DDR in the cerebellar VZ, and resort to NHEJ for DNA repair. This increase is more evident in the Δ9-20 mutant, in keeping the precocious differentiation of VZ progenitors observed in this mutant.

Taken together, these results strongly suggest that in both *Zfp423* mutants the frequency of double-strand breaks is significantly increased throughout the cell cycle, likely due to inefficient repair. This causes a comparably sharp increase in residual DNA damage in differentiating neurons.

DISCUSSION

The key role played by *Zfp423/ZNF423* in cerebellar morphogenesis has been addressed through the analysis of mouse models and human patients. Studies conducted on mouse lines carrying null mutations of *Zfp423* have pinpointed the importance of this gene in cerebellar organogenesis (Alcaraz et al., 2006; Cheng et al., 2007; Warming et al., 2006). Moreover, through a combined homozygosity mapping and exome analysis approaches, mutations of *ZNF423* have been identified in Joubert syndrome and in individuals with nephronophthisis, classifying *ZNF423* as a human ciliopathy gene (Chaki et al., 2012). All JS proteins identified prior to this discovery are primary cilium or basal body components. However, the evidence supporting a centrosomal localization of

Development (2017) 144, 3686-3697 doi:10.1242/dev.155077

ZFP423 is still inconclusive. In our hands, ZFP423 is clearly localized in the cell nucleus, in agreement with its established role as a transcription factor (Hata et al., 2000; Ku et al., 2003, 2006; Masserdotti et al., 2010; Tsai and Reed, 1997, 1998).

The role of the cilium in GC development (Chizhikov et al., 2007) relates to the function of this organelle in SHH signaling and other regulatory pathways. Other authors have demonstrated that ZFP423 regulates the proliferative response of GC progenitors to SHH (Hong and Hamilton, 2016). However, our work also implicates ZFP423 in the control of PC development, which is independent of SHH signaling. The role, if any, of the primary cilium in this process has not been addressed to date. Incidentally, the overall number of GCs in the mouse cerebellum is determined by the number of immature PCs releasing SHH between the late fetal period and postnatal day 15, linking the two processes (Dahmane and Ruiz-i-Altaba, 1999; Wallace, 1999; Wechsler-Reya and Scott, 1999). Thus, the cerebellar hypoplasia observed in our mutants is most likely a combination of PC- and GC-progenitor proliferation defects.

In humans, JS can be clearly diagnosed as a cerebellar malformation *in utero* by magnetic resonance imaging (Saleem et al., 2011), while the bulk of GC clonal expansion occurs after birth in humans (Kiessling et al., 2014) as in mice. JS research has dealt more with GCs than with PCs in both human patients and murine models. To fill this gap, we have focused on early stages of PC development. Our findings indicate that the two allelic deletions have divergent effects on PC progenitor pool maintenance, PC progenitor differentiation and cerebellar cortical patterning. Conversely, both *Zfp423* deletions analyzed here cause a delay in PC progenitor cell cycle progression, and a significant increase in the number of mitotic and postmitotic precursors positive for DNA-damage markers.

The Δ9-20 mutation affects the maintenance of mitotic PC progenitors

The two mouse lines analyzed in this work carry distinct functionally characterized ZFP423 protein domains. The two mutations, while both giving rise to stable nuclear proteins, do not produce any detectable gain of function: in fact, heterozygotes are morphologically and functionally normal, whereas homozygotes have cerebellar hypoplasia and are severely ataxic (not shown). Our findings uncover some specific roles in PC development for each of the deleted ZFP423 protein domains. The deletion of the domain spanning zinc fingers 9-20 causes a precocious depletion of proliferating OLIG2^{+} progenitors in the VZ (Fig. 4A), which translates into a depletion of PLCβ4^{+} PCs, mostly late born, whereas early-born PCs (mostly zebrinII+) are relatively spared (Fig. 3C). As a result, the alternating pattern of zebrinII^{+} and zebrinII^{-} stripes is lost in the Δ9-20 cerebellum and maintained in the Δ28-30 cerebellum, despite its small size. In keeping with this observation, at E11.5, the Δ9-20 cerebellar VZ displays changes in M-phase progenitor spindle orientation, suggesting an increased propensity towards neurogenic cell division (Fig. 5B). This is also confirmed by our *in vitro* results: in the cell pair assay (Bultje et al., 2009), this change translates into an increase in the ratio of neurogenic to proliferative cell divisions in Δ9-20 NEPs, which is not observed in Δ28-30 NEPs (Fig. 5E). Incidentally, because ZFP423 signal peaks in M-phase VZ progenitors, and appears to colocalize with nuclear membrane components implicated in mitotic spindle organization (lamin B, Kim et al., 2011b) (Fig. 1E) and to segregate from compacted chromatin, the possibility of a transcription-independent role of this protein in regulating spindle orientation cannot be excluded, and should be addressed experimentally.

Zinc fingers 28-30 of ZFP423 regulate PC progenitor differentiation

In contrast with the observations made in the Δ9-20 primordium, in the Δ28-30 mutant, OLIG2^{+} progenitors are not decreased in number, in keeping with the fact that late-born PCs are present in this strain, while levels of CORL2 and *Lhx5*, both markers of early PC differentiation, are strikingly reduced (see Fig. 4B,C). The C-terminal domain of ZFP423 mediates the interaction of this protein with EBF transcription factors (Hata et al., 2000; Masserdotti et al., 2010; Tsai and Reed, 1997, 1998), which play a key role in coupling cell cycle exit with the onset of neuronal migration and differentiation in neural tube development (Garcia-Dominguez et al., 2003). Two EBF transcription factors, EBF2 and EBF3 (Malgaretti et al., 1997; Wang et al., 1997), have been implicated in mouse and human cerebellar development, respectively (Chao et al., 2017; Chung et al., 2008; Croci et al., 2006; Harms et al., 2017; Sleven et al., 2017). EBF2, in particular, affects various aspects of PC development, namely the migration and survival of a late-born PC subset. In the Δ28-30 mutant, PC progenitor differentiation may be delayed or impaired due to the lack of ZFP423-EBF interaction. However, the deletion of zinc fingers 9-20 does not affect the interaction of ZFP423 with EBF transcription factors, but may recruit ZFP423 into an inactive heterodimer with EBF, shifting the balance from progenitor maintenance to the onset of differentiation, promoted by EBF-EBF homodimers.

Although ZFP423 is expressed at robust levels in VZ progenitors, suggesting a cell-autonomous role of this protein, it is also found in rhombic lip and roof-plate derivatives. While there is no known effect of RL progenitors on PC development prior to PC migration, extracellular factors secreted by the roof plate and choroid plexus may possibly contribute to the alterations observed in our mutants. Conditional inactivation of *Zfp423* in different lineages should provide answers to these open questions.

Both ZFP423 deletions cause cell cycle progression arrest in a subset of G2 cells

In this work, we studied cell cycle progression in our mutant lines by analyzing the expression of global and cell type-specific markers. DNA replication was assessed by a single 30′ EdU pulse at E12.5. At this stage, the S/M and G_2/M ratios were significantly increased in both mutants (Fig. 6A,B), suggesting that some cells are delayed in their progression from S to M. Given the role of ZFP423 in the DDR (Chaki et al., 2012), we speculated that ZFP423 mutation might cause a subset of progenitors to stall during the same interval. In particular, the delay in G_2-M progression strongly suggests that ZFP423, which is expressed at very low levels in G_1 progenitors (Fig. S1A), is involved in permitting transition through the G_2-M cell cycle checkpoint. This evidence prompted an *in vivo* analysis of DNA damage in PC progenitors.

Both ZFP423 deletions cause an increase in ds-DNA-damage signaling in the cerebellar primordium

Although each deletion affects separate aspects of PC progenitor development, both mutants show a massive increase in ds-DNA-damage signaling in the cerebellar VZ. The 9-20 domain of ZFP423 overlaps almost entirely with the region of the protein known to interact with the dsDNA-damage sensor PARP1 (poly-ADP ribosyl polymerase 1) (Ku et al., 2003). PARP1 decreases the affinity of the Ku70-Ku80 heterodimer for ds breaks, permitting end resection and shifting the balance of DNA repair from NHEJ to HR (Hochegger et al., 2006). In the context of the DDR, HR occurs, by definition,

Development (2017) 144, 3686-3697 doi:10.1242/dev.155077

after DNA replication, to recruit a homologous chromatid (usually a sister chromatid) as a template for DNA repair. In order for HR-mediated repair to occur, cell cycle progression must be arrested so as to delay chromatin compaction, which would make the search for homology difficult. Our evidence suggests that DNA-damage signaling is significantly increased in S-M progenitors (Fig. 6A). Conceivably, in the Δ9-20 cerebellum, which loses the PARP1 interaction domain, a defective recruitment of PARP1 could prevent the assembly of a functional DNA repair complex acting between S and M, presumably by HR. Although zinc fingers 9-20 contain the PARP1 interaction domain and are immediately adjacent to the CEP290 interaction site (Chaki et al., 2012), no clues are available to date regarding the possible function of zinc fingers 28-30 in the context of DNA repair. We hypothesize that the integrity of the ZFP423 C-terminus is necessary to assemble a functional DNA repair complex with as yet unidentified co-factors. Possibly because of the diminished efficiency of HR in mitotic cells, both mutants sharply upregulate the DNA end resection inhibitor 53BP1 (Escribano-Díaz et al., 2013) in postmitotic CTZ precursors, which are strictly dependent on NHEJ for dsDNA repair.

Ciliopathy genes, the DDR and Joubert syndrome

The finding of a highly significant increase in endogenous dsDNA damage in cycling VZ neural progenitors further supports the emerging notion that several ciliopathy genes play important extra-ciliary roles in the nucleus, participating in the DDR. This has been shown elegantly in renal ciliopathies: both *CEP290* and *NEK8* mutations (Choi et al., 2013; Slaats et al., 2015) lead to an accumulation of DNA damage due to disturbed replication forks. Furthermore, increased DNA-damage signaling has been scored in *CEP164*-, *ZNF423*- and *SDCCAG8*-associated nephronophthisis (Hochegger et al., 2006). This study raises the possibility that cerebellar hypoplasia in JS, and in other cerebellar malformations, may stem at least partially from defective DNA repair and consequent cell cycle delay. In conclusion, the evidence of an impairment in cell cycle progression/exit and endogenous DNA-damage repair in fast-cycling cerebellar VZ progenitors furthers our understanding of JS, and may have far reaching implications in our overall approach to this elusive disorder.

MATERIALS AND METHODS

Animal care

All experiments described in this paper were performed in agreement with the stipulations of the San Raffaele Scientific Institute Animal Care and Use Committee (I.A.C.U.C.) and the Guide to the Care and Use of Experimental Animals from the Canadian Council for Animal Care.

Mouse genetics

The *Zfp423* Δ9-20 and Δ28-30 mouse lines were generated by gene targeting. The targeting constructs were engineered using BAC recombineering in *E. coli*; the mutations were introduced into the *Zfp423* gene by homologous recombination in 129S1/SVImJ cells. The resulting mutants were then backcrossed repeatedly with C57BL/6N mice to generate congenic strains. All experiments were carried out on homozygous mutant animals starting from backcross generation N8, expected to carry 99.6% of the C57BL/6N genetic background. All studies were conducted in homozygous mutant embryos of either sex, using co-isogenic wild-type control littermates. Genotyping was carried by PCR as described previously (Corradi et al., 2003) using allele-specific primers.

Western blotting

P0 cerebella were homogenized in ice-cold RIPA buffer containing protease inhibitors, 10 mM DTT and 8 M urea, and treated with 100 U of benzonase nuclease (Sigma). The extracts were incubated in sample buffer [50 mM Tris-HCl (pH 6.8), 2% SDS, 33 mM DTT, 0.1 M β-mercaptoethanol, 8 M urea, 10% glycerol, 0.1% Bromophenol blue] for 10 min at room temperature. After gel electrophoresis on a 10% SDS-polyacrylamide gel (Biorad), proteins were transferred onto a nitrocellulose membrane (Biorad). Western blotting was performed with a rabbit polyclonal anti-Zfp423 (1:1000, Santa Cruz sc-48785, amino acids 1-105) (validated by Hong and Hamilton, 2016; Shao et al., 2016) and a mouse monoclonal anti-β-actin (1:5000, Sigma) antibodies.

Tissue preparation

Pregnant dams were anesthetized using Avertin (Sigma) prior to cervical dislocation. Embryos were fixed for 6-8 h by immersion with 4% PFA in 1× PBS, cryoprotected overnight in 30% sucrose in 1× PBS, embedded in OCT (Bioptica) and stored at −80°C. For postnatal brains, mice were anesthetized with Avertin (Sigma), transcardially perfused with 0.9% NaCl, followed by 4% PFA in 1× PBS and prepared for freezing as above. The brains and embryos were sectioned sagittally or frontally on a cryotome.

EdU administration and labeling

Pregnant dams were injected intraperitoneally with 5-ethynyl-2′-deoxyuridine (EdU, 50 µg/g body weight). Embryos were collected and treated as described above. EdU incorporation was revealed using the Click-iT EdU Cell Proliferation Assay kit (Life Technologies), according to the manufacturer's instructions.

Immunofluorescence and TUNEL staining

Sections were washed in 1× PBS, blocked and permeabilized in 10% serum, 0.3% Triton X-100 in 1× PBS and incubated with primary antibodies overnight at 4°C, rinsed, then incubated with secondary antibodies at room temperature for 2 h (1:1000 Alexa Fluor, Molecular Probes). Sections were counterstained with 4′,6-diamidino-2-phenylindole (DAPI, 1:5000, Sigma) and mounted with fluorescent mounting medium (Dako). Peroxidase immunohistochemistry was performed as described previously (Sarna et al., 2006). TUNEL assays were performed using ApopTag kit (Millipore) according to the manufacturer's instructions.

In situ hybridization

Digoxigenin-labeled riboprobes were transcribed from plasmids containing *Lhx5* cDNAs. *In situ* hybridization was performed as described previously (Croci et al., 2011).

Analysis of mitotic cleavage plane orientation and distribution of apical membrane in VZ progenitors

E11.5 sections were stained for PHH3 and pancadherin, and counterstained with DAPI. DAPI and PHH3 were used to identify mitotic cells in anaphase/early telophase. For each mitotic cell, we took three consecutive confocal images (1 µm intervals). To determine the cleavage plane, we drew two rectangles, each containing one of the two sets of sister chromatids; cleavage planes were classified based on their angle with respect to the ventricular surface. To designate mitoses as equal versus unequal, we took into account the orientation of the cleavage plane and its position with respect to the so-called cadherin hole, i.e. the gap within the apical adherens junction observed in dividing radial glia (see sample images in Fig. 5A) (for exact criteria, see Kosodo et al., 2004).

Cell pair assay

E11.5 cerebellar primordia were dissected in HBSS, collected by centrifugation and dissociated by pipetting in culture medium containing DMEM (Sigma), glutamax (Life Technologies), penicillin/streptomycin (Euroclone), 1 mM sodium pyruvate (Life Technologies), 1 mM N-acetyl-L-cysteine (Sigma), B27 and N2 (Life Technologies), and 10 ng/ml FGF2 (Peprotech). Single cells were plated onto 24-well plates coated with poly-D-lysine (10 µg/ml), at a density of 30,000 cells/well. The cultures were maintained in a humidified incubator at 37°C with constant 5% CO_2 supply. About 24 h later, the cultures were fixed and immunostained using anti-βIII-Tubulin (1:500, Covance, MMS-435P) and anti-Sox2 (1:250, Abcam, ab59776) Abs, and counterstained with DAPI (Sigma).

Development (2017) 144, 3686-3697 doi:10.1242/dev.155077

Approximately 50 images per well were acquired using the GE Healthcare IN Cell Analyzer 1000 and analyzed with Adobe Photoshop.

RT-qPCR

Total RNA was extracted with RNeasy MiniKit (Qiagen), according to manufacturer's instructions. Total RNA (1-1.5 µg) was retrotranscribed using first-strand cDNA MMLV-retrotranscriptase (Invitrogen) and random primers. Each cDNA was diluted 1:10 and 3 µl were used for each RT-qPCR reaction. mRNA quantitation was performed with SYBR Green I Master Mix (Roche) on a LightCycler480 instrument (Roche). Each gene was analyzed in triplicate and each experiment was repeated at least three times. Data analysis was performed with the 2-ΔΔC(T) method. All RNA levels were normalized based upon β-actin, *H3f3a and Gapdh* transcript levels.

Primer sequences

Genotyping primers were as follows: *Δ9-20*-wtF, 5′-GGCTTCCATGAGC-AGTGCT-3′; *Δ9-20*-wtR, 5′-CTCCTGCAGGCTGTTGATGT-3′; *Δ9-20*-mutR, 5′-CGTCCACGTCATCCTCACT-3′; *Δ28-30*-wtF, 5′-TGAGAGAG-GACACCTACTCT-3′; *Δ28-30*-wtR, 5′-GCAGGGAGCAAACTGTCTCT-T-3′; *Δ28-30*-mutR, 5′-GGTGTGACCTTTGTGCGAGA-3′.

RT-qPCR primers were as follows: *Zfp423* F, 5′-CTTCTCGCTGGCCT-GGGATT-3′; *Zfp423* R, 5′- GGTCTGCCAGAGACTCGAAGT-3′; *β-actin* F, 5′-CTGTCGAGTCGCGTCCACC-3′; *β-actin* R, 5′-TCGTCATCCATG-GCGAACTG-3′; *H3f3a* F, 5′-GGTGAAGAAACCTCATCGTTACAGGC-CTGGTAC-3′; *H3f3a* R, 5′-CTGCAAAGCACCAATAGCTGCACTCT-GGAAGC-3′; *Gapdh* F, 5′-TGAAGCAGGCATCTGAGGG-3′; *Gapdh* R, 5′-CGAAGGTGGAAGAGTGGGAG-3′.

Antibodies

Mouse monoclonal antibodies used were: pan-cadherin (1:300, Sigma, C1821); βIII-tubulin (1:500, Covance, MMS-435P); zebrin II (Brochu et al., 1990), used in spent hybridoma supernatant (1:5000); phospho-histone H3 (1:1000, Abcam, ab14955); and OLIG2 (1:200, Millipore, MAB50). Rabbit antibodies included: calbindin (1:1000, Swant, CB-38a); ZFP423/OAZ XL (1:1000, Santa Cruz Biotechnology, sc48785); FOXP2 (1:1000, Abcam, ab16046); phospho-histone H3 (1:800, monoclonal, Millipore, 06-570); phospholipase Cβ4 (PLCβ4) (1:1000, a kind gift from Dr M. Watanabe, Hokkaido University, Japan); SOX2 (1:250, Abcam, ab59776); SOX9 (1:2000, Millipore, AB5535); OLIG2 (1:500, Millipore, AB9610); CORL2 (1:2000, Aviva System Biology, OAAB18965); γ-H2AX (1:200, Cell Signaling, 9718); and 53BP1 (1:1000, Bethyl Lab, A300-272A). LaminB goat antibody was used (1:100, Santa Cruz, sc-6216). Signal from anti-OAZ antibodies was amplified using the Tyramide Signal Amplification Kit (Perkin Elmer), according to manufacturer's instructions. Cells were immunostained using the ZFP423 antibody used in all experiments shown in this paper (Santa Cruz, sc-48785, amino acids 1-105; Fig. S4).

Microscopy and image processing

Optical microscopy was carried out using a Leica SP8 microscope or a Zeiss AxioImager M2m microscope. Digital images were processed with Adobe Photoshop to adjust contrast and brightness according to Journal's recommendations. Quantitative and morphometric evaluations were performed using the ImageJ software (NIH). In Fig. 6C,D, signal was quantitated as the ratio of the area occupied by γH2AX to that occupied by DAPI (C), or EdU^{3h} (D). Quantitation was achieved with ImageJ using the selection tool to delimit areas of interest.

Statistical analysis

All experiments were conducted on a minimum of three biological replicates, represented by coisogenic mice/embryos, except where noted. Statistical analysis was performed in Graphpad Prism and was conducted as follows: a) the two-tailed unequal variance *t*-test (Welch's *t*-test) was employed to compare sets of quantitative values (wild type versus each mutant), b) categorical values were analyzed by means of the two-tailed Fisher's exact test, and plotted as proportions, percentages or actual numbers, c) one-way ANOVA was calculated through the Kruskal–Wallis test followed by Dunn's post hoc test for the comparison of areas occupied by different signals.

Acknowledgements

Image analysis was carried out in ALEMBIC, an advanced microscopy laboratory established by the San Raffaele Scientific Institute and Vita-Salute San Raffaele University. We thank F. Bani and G. Bergamini for their contribution to this project.

Competing interests

The authors declare no competing or financial interests.

Author contributions

Conceptualization: F.C., L.C., O.C., G.G.C.; Methodology: L.T., S.W., G.G.C.; Formal analysis: F.C., D.G., G.G.C.; Investigation: F.C., L.C., C.B., R.D., A.B., V.B., J.R.S., R.H.; Writing - original draft: F.C., L.C., G.G.C.; Writing - review & editing: F.C., L.C., O.C., R.H., S.W., G.G.C.; Visualization: F.C., L.C., R.D.; Supervision: G.G.C.; Project administration: G.G.C.; Funding acquisition: G.G.C.

Funding

This work was mostly funded by the Fondazione Telethon (GGP13146 to G.G.C.); an additional contribution was provided by Ministero della Salute Ricerca Finalizzata 2011 (PE-2011-02347716 to O.C.). R.H. was supported by an award from the Canadian Institutes of Health Research. S.W. and L.T. were supported by the National Institutes of Health Intramural Research Program, Center for Cancer Research, National Cancer Institute. Deposited in PMC for release after 12 months.

Supplementary information

Supplementary information available online at
http://dev.biologists.org/lookup/doi/10.1242/dev.155077.supplemental

References

Airik, R., Slaats, G. G., Guo, Z., Weiss, A.-C., Khan, N., Ghosh, A., Hurd, T. W., Bekker-Jensen, S., Schroder, J. M., Elledge, S. J. et al. (2014). Renal-retinal ciliopathy gene Sdccag8 regulates DNA damage response signaling. *J. Am. Soc. Nephrol.* **25**, 2573-2583.

Alcaraz, W. A., Gold, D. A., Raponi, E., Gent, P. M., Concepcion, D. and Hamilton, B. A. (2006). Zfp423 controls proliferation and differentiation of neural precursors in cerebellar vermis formation. *Proc. Natl. Acad. Sci. USA* **103**, 19424-19429.

Alcaraz, W. A., Chen, E., Valdes, P., Kim, E., Lo, Y. H., Vo, J. and Hamilton, B. A. (2011). Modifier genes and non-genetic factors reshape anatomical deficits in Zfp423-deficient mice. *Hum. Mol. Genet.* **20**, 3822-3830.

Aldinger, K. A., Lehmann, O. J., Hudgins, L., Chizhikov, V. V., Bassuk, A. G., Ades, L. C., Krantz, I. D., Dobyns, W. B. and Millen, K. J. (2009). FOXC1 is required for normal cerebellar development and is a major contributor to chromosome 6p25.3 Dandy-Walker malformation. *Nat. Genet.* **41**, 1037-1042.

Anthony, T. E., Klein, C., Fishell, G. and Heintz, N. (2004). Radial glia serve as neuronal progenitors in all regions of the central nervous system. *Neuron* **41**, 881-890.

Branzei, D. and Foiani, M. (2008). Regulation of DNA repair throughout the cell cycle. *Nat. Rev. Mol. Cell Biol.* **9**, 297-308.

Brochu, G., Maler, L. and Hawkes, R. (1990). Zebrin II: a polypeptide antigen expressed selectively by Purkinje cells reveals compartments in rat and fish cerebellum. *J. Comp. Neurol.* **291**, 538-552.

Bultje, R. S., Castaneda-Castellanos, D. R., Jan, L. Y., Jan, Y.-N., Kriegstein, A. R. and Shi, S.-H. (2009). Mammalian Par3 regulates progenitor cell asymmetric division via notch signaling in the developing neocortex. *Neuron* **63**, 189-202.

Celeste, A., Petersen, S., Romanienko, P. J., Fernandez-Capetillo, O., Chen, H. T., Sedelnikova, O. A., Reina-San-Martin, B., Coppola, V., Meffre, E., Difilippantonio, M. J. et al. (2002). Genomic instability in mice lacking histone H2AX. *Science* **296**, 922-927.

Chaki, M., Airik, R., Ghosh, A. K., Giles, R. H., Chen, R., Slaats, G. G., Wang, H., Hurd, T. W., Zhou, W., Cluckey, A. et al. (2012). Exome capture reveals ZNF423 and CEP164 mutations, linking renal ciliopathies to DNA damage response signaling. *Cell* **150**, 533-548.

Chao, H.-T., Davids, M., Burke, E., Pappas, J. G., Rosenfeld, J. A., McCarty, A. J., Davis, T., Wolfe, L., Toro, C., Tifft, C. et al. (2017). A syndromic neurodevelopmental disorder caused by de novo variants in EBF3. *Am. J. Hum. Genet.* **100**, 128-137.

Cheng, L. E., Zhang, J. and Reed, R. R. (2007). The transcription factor Zfp423/OAZ is required for cerebellar development and CNS midline patterning. *Dev. Biol.* **307**, 43-52.

Chizhikov, V. V., Lindgren, A. G., Currle, D. S., Rose, M. F., Monuki, E. S. and Millen, K. J. (2006). The roof plate regulates cerebellar cell-type specification and proliferation. *Development* **133**, 2793-2804.

Chizhikov, V. V., Davenport, J., Zhang, Q., Shih, E. K., Cabello, O. A., Fuchs, J. L., Yoder, B. K. and Millen, K. J. (2007). Cilia proteins control cerebellar morphogenesis by promoting expansion of the granule progenitor pool. *J. Neurosci.* **27**, 9780-9789.

Development (2017) 144, 3686-3697 doi:10.1242/dev.155077

Cho, Y.-W., Hong, C.-J., Hou, A., Gent, P. M., Zhang, K., Won, K.-J. and Hamilton, B. A. (2013). Zfp423 binds autoregulatory sites in p19 cell culture model. *PLoS ONE* **8**, e66514.

Choi, H. J. C., Lin, J.-R., Vannier, J.-B., Slaats, G. G., Kile, A. C., Paulsen, R. D., Manning, D. K., Beier, D. R., Giles, R. H., Boulton, S. J. et al. (2013). NEK8 links the ATR-regulated replication stress response and S phase CDK activity to renal ciliopathies. *Mol. Cell* **51**, 423-439.

Chung, S.-H., Marzban, H., Croci, L., Consalez, G. G. and Hawkes, R. (2008). Purkinje cell subtype specification in the cerebellar cortex: early B-cell factor 2 acts to repress the Zebrin II-positive Purkinje cell phenotype. *Neuroscience* **153**, 721-732.

Chung, S.-H., Sillitoe, R. V., Croci, L., Badaloni, A., Consalez, G. and Hawkes, R. (2009). Purkinje cell phenotype restricts the distribution of unipolar brush cells. *Neuroscience* **164**, 1496-1508.

Corradi, A., Croci, L., Broccoli, V., Zecchini, S., Previtali, S., Wurst, W., Amadio, S., Maggi, R., Quattrini, A. and Consalez, G. G. (2003). Hypogonadotropic hypogonadism and peripheral neuropathy in Ebf2-null mice. *Development* **130**, 401-410.

Croci, L., Chung, S. H., Masserdotti, G., Gianola, S., Bizzoca, A., Gennarini, G., Corradi, A., Rossi, F., Hawkes, R. and Consalez, G. G. (2006). A key role for the HLH transcription factor EBF2COE2,O/E-3 in Purkinje neuron migration and cerebellar cortical topography. *Development* **133**, 2719-2729.

Croci, L., Barili, V., Chia, D., Massimino, L., van Vugt, R., Masserdotti, G., Longhi, R., Rotwein, P. and Consalez, G. G. (2011). Local insulin-like growth factor I expression is essential for Purkinje neuron survival at birth. *Cell Death Differ.* **18**, 48-59.

Dahmane, N. and Ruiz-i-Altaba, A. (1999). Sonic hedgehog regulates the growth and patterning of the cerebellum. *Development* **126**, 3089-3100.

Escribano-Díaz, C., Orthwein, A., Fradet-Turcotte, A., Xing, M., Young, J. T. F., Tkáč, J., Cook, M. A., Rosebrock, A. P., Munro, M., Canny, M. D. et al. (2013). A cell cycle-dependent regulatory circuit composed of 53BP1-RIF1 and BRCA1-CtIP controls DNA repair pathway choice. *Mol. Cell* **49**, 872-883.

Fish, J. L., Kosodo, Y., Enard, W., Paabo, S. and Huttner, W. B. (2006). Aspm specifically maintains symmetric proliferative divisions of neuroepithelial cells. *Proc. Natl. Acad. Sci. USA* **103**, 10438-10443.

Florio, M., Leto, K., Muzio, L., Tinterri, A., Badaloni, A., Croci, L., Zordan, P., Barili, V., Albieri, I., Guillemot, F. et al. (2012). Neurogenin 2 regulates progenitor cell-cycle progression and Purkinje cell dendritogenesis in cerebellar development. *Development* **139**, 2308-2320.

Garcia-Dominguez, M., Poquet, C., Garel, S. and Charnay, P. (2003). Ebf gene function is required for coupling neuronal differentiation and cell cycle exit. *Development* **130**, 6013-6025.

Gertz, C. C., Lui, J. H., LaMonica, B. E., Wang, X. and Kriegstein, A. R. (2014). Diverse behaviors of outer radial glia in developing ferret and human cortex. *J. Neurosci.* **34**, 2559-2570.

Goetz, S. C. and Anderson, K. V. (2010). The primary cilium: a signalling centre during vertebrate development. *Nat. Rev. Genet.* **11**, 331-344.

Goldowitz, D. and Hamre, K. (1998). The cells and molecules that make a cerebellum. *Trends Neurosci.* **21**, 375-382.

Götz, M. and Huttner, W. B. (2005). The cell biology of neurogenesis. *Nat. Rev. Mol. Cell Biol.* **6**, 777-788.

Grimaldi, P., Parras, C., Guillemot, F., Rossi, F. and Wassef, M. (2009). Origins and control of the differentiation of inhibitory interneurons and glia in the cerebellum. *Dev. Biol.* **328**, 422-433.

Han, Y.-G. and Alvarez-Buylla, A. (2010). Role of primary cilia in brain development and cancer. *Curr. Opin. Neurobiol.* **20**, 58-67.

Harms, F. L., Girisha, K. M., Hardigan, A. A., Kortüm, F., Shukla, A., Alawi, M., Dalal, A., Brady, L., Tarnopolsky, M., Bird, L. M. et al. (2017). Mutations in EBF3 disturb transcriptional profiles and cause intellectual disability, ataxia, and facial dysmorphism. *Am. J. Hum. Genet.* **100**, 117-127.

Hashimoto, M. and Mikoshiba, K. (2003). Mediolateral compartmentalization of the cerebellum is determined on the "birth date" of Purkinje cells. *J. Neurosci.* **23**, 11342-11351.

Hata, A., Seoane, J., Lagna, G., Montalvo, E., Hemmati-Brivanlou, A. and Massagué, J. (2000). OAZ uses distinct DNA- and protein-binding zinc fingers in separate BMP-Smad and Olf signaling pathways. *Cell* **100**, 229-240.

Hochegger, H., Dejsuphong, D., Fukushima, T., Morrison, C., Sonoda, E., Schreiber, V., Zhao, G. Y., Saberi, A., Masutani, M., Adachi, N. et al. (2006). Parp-1 protects homologous recombination from interference by Ku and Ligase IV in vertebrate cells. *EMBO J.* **25**, 1305-1314.

Hong, C.-J. and Hamilton, B. A. (2016). Zfp423 regulates sonic hedgehog signaling via primary cilium function. *PLoS Genet.* **12**, e1006357.

Hoshino, M., Nakamura, S., Mori, K., Kawauchi, T., Terao, M., Nishimura, Y. V., Fukuda, A., Fuse, T., Matsuo, N., Sone, M. et al. (2005). Ptf1a, a bHLH transcriptional gene, defines GABAergic neuronal fates in cerebellum. *Neuron* **47**, 201-213.

Ju, J., Liu, Q., Zhang, Y., Liu, Y., Jiang, M., Zhang, L., He, X., Peng, C., Zheng, T., Lu, Q. R. et al. (2016). Olig2 regulates Purkinje cell generation in the early developing mouse cerebellum. *Sci. Rep.* **6**, 30711.

Kiessling, M. C., Büttner, A., Butti, C., Müller-Starck, J., Milz, S., Hof, P. R., Frank, H.-G. and Schmitz, C. (2014). Cerebellar granule cells are generated postnatally in humans. *Brain Struct. Funct.* **219**, 1271-1286.

Kim, E. J., Hori, K., Wyckoff, A., Dickel, L. K., Koundakjian, E. J., Goodrich, L. V. and Johnson, J. E. (2011a). Spatiotemporal fate map of neurogenin1 (Neurog1) lineages in the mouse central nervous system. *J. Comp. Neurol.* **519**, 1355-1370.

Kim, Y., Sharov, A. A., McDole, K., Cheng, M., Hao, H., Fan, C.-M., Gaiano, N., Ko, M. S. H. and Zheng, Y. (2011b). Mouse B-type lamins are required for proper organogenesis but not by embryonic stem cells. *Science* **334**, 1706-1710.

Kosodo, Y., Röper, K., Haubensak, W., Marzesco, A.-M., Corbeil, D. and Huttner, W. B. (2004). Asymmetric distribution of the apical plasma membrane during neurogenic divisions of mammalian neuroepithelial cells. *EMBO J.* **23**, 2314-2324.

Ku, M. C., Stewart, S. and Hata, A. (2003). Poly(ADP-ribose) polymerase 1 interacts with OAZ and regulates BMP-target genes. *Biochem. Biophys. Res. Commun.* **311**, 702-707.

Ku, M., Howard, S., Ni, W., Lagna, G. and Hata, A. (2006). OAZ regulates bone morphogenetic protein signaling through Smad6 activation. *J. Biol. Chem.* **281**, 5277-5287.

Larouche, M. and Hawkes, R. (2006). From clusters to stripes: the developmental origins of adult cerebellar compartmentation. *Cerebellum* **5**, 77-88.

Leto, K., Carletti, B., Williams, I. M., Magrassi, L. and Rossi, F. (2006). Different types of cerebellar GABAergic interneurons originate from a common pool of multipotent progenitor cells. *J. Neurosci.* **26**, 11682-11694.

Leto, K., Bartolini, A., Yanagawa, Y., Obata, K., Magrassi, L., Schilling, K. and Rossi, F. (2009). Laminar fate and phenotype specification of cerebellar GABAergic interneurons. *J. Neurosci.* **29**, 7079-7091.

Leto, K., Arancillo, M., Becker, E. B., Buffo, A., Chiang, C., Ding, B., Dobyns, W. B., Dusart, I., Haldipur, P., Hatten, M. E. et al. (2015). Consensus paper: cerebellar development. *Cerebellum* **15**, 789-828.

Li, H.-S., Wang, D., Shen, Q., Schonemann, M. D., Gorski, J. A., Jones, K. R., Temple, S., Jan, L. Y. and Jan, Y. N. (2003). Inactivation of Numb and Numblike in embryonic dorsal forebrain impairs neurogenesis and disrupts cortical morphogenesis. *Neuron* **40**, 1105-1118.

Lundell, T. G., Zhou, Q. and Doughty, M. L. (2009). Neurogenin1 expression in cell lineages of the cerebellar cortex in embryonic and postnatal mice. *Dev. Dyn.* **238**, 3310-3325.

Lütolf, S., Radtke, F., Aguet, M., Suter, U. and Taylor, V. (2002). Notch1 is required for neuronal and glial differentiation in the cerebellum. *Development* **129**, 373-385.

Machold, R. P., Kittell, D. J. and Fishell, G. J. (2007). Antagonism between Notch and bone morphogenetic protein receptor signaling regulates neurogenesis in the cerebellar rhombic lip. *Neural Dev.* **2**, 5.

Malgaretti, N., Pozzoli, O., Bosetti, A., Corradi, A., Ciarmatori, S., Panigada, M., Bianchi, M. E., Martinez, S. and Consalez, G. G. (1997). Mmot1, a new helix-loop-helix transcription factor gene displaying a sharp expression boundary in the embryonic mouse brain. *J. Biol. Chem.* **272**, 17632-17639.

Maricich, S. M. and Herrup, K. (1999). Pax-2 expression defines a subset of GABAergic interneurons and their precursors in the developing murine cerebellum. *J. Neurobiol.* **41**, 281-294.

Massagué, J. (2000). How cells read TGF-beta signals. *Nat. Rev. Mol. Cell Biol.* **1**, 169-178.

Masserdotti, G., Badaloni, A., Green, Y. S., Croci, L., Barili, V., Bergamini, G., Vetter, M. L. and Consalez, G. G. (2010). ZFP423 coordinates Notch and bone morphogenetic protein signaling, selectively up-regulating Hes5 gene expression. *J. Biol. Chem.* **285**, 30814-30824.

McKinnon, P. J. (2013). Maintaining genome stability in the nervous system. *Nat. Neurosci.* **16**, 1523-1529.

Minaki, Y., Nakatani, T., Mizuhara, E., Inoue, T. and Ono, Y. (2008). Identification of a novel transcriptional corepressor, Corl2, as a cerebellar Purkinje cell-selective marker. *Gene Expr. Patterns* **8**, 418-423.

Mizuhara, E., Minaki, Y., Nakatani, T., Kumai, M., Inoue, T., Muguruma, K., Sasai, Y. and Ono, Y. (2009). Purkinje cells originate from cerebellar ventricular zone progenitors positive for Neph3 and E-cadherin. *Dev. Biol.* **338**, 202-214.

Panier, S. and Boulton, S. J. (2014). Double-strand break repair: 53BP1 comes into focus. *Nat. Rev. Mol. Cell Biol.* **15**, 7-18.

Romani, M., Micalizzi, A. and Valente, E. M. (2013). Joubert syndrome: congenital cerebellar ataxia with the molar tooth. *Lancet Neurol.* **12**, 894-905.

Roussel, M. F. and Hatten, M. E. (2011). Cerebellum development and medulloblastoma. *Curr. Top. Dev. Biol.* **94**, 235-282.

Saleem, S. N., Zaki, M. S., Soliman, N. A. and Momtaz, M. (2011). Prenatal magnetic resonance imaging diagnosis of molar tooth sign at 17 to 18 weeks of gestation in two fetuses at risk for Joubert syndrome and related cerebellar disorders. *Neuropediatrics* **42**, 35-38.

Salsano, E., Croci, L., Maderna, E., Lupo, L., Pollo, B., Giordana, M. T., Consalez, G. G. and Finocchiaro, G. (2007). Expression of the neurogenic basic helix-loop-helix transcription factor NEUROG1 identifies a subgroup of medulloblastomas not expressing ATOH1. *Neuro Oncol.* **9**, 298-307.

Sarna, J. R., Marzban, H., Watanabe, M. and Hawkes, R. (2006). Complementary stripes of phospholipase Cbeta3 and Cbeta4 expression by Purkinje cell subsets in the mouse cerebellum. *J. Comp. Neurol.* **496**, 303-313.

Seto, Y., Nakatani, T., Masuyama, N., Taya, S., Kumai, M., Minaki, Y., Hamaguchi, A., Inoue, Y. U., Inoue, T., Miyashita, S. et al. (2014). Temporal identity transition from Purkinje cell progenitors to GABAergic interneuron progenitors in the cerebellum. *Nat. Commun.* **5**, 3337.

Shao, M., Ishibashi, J., Kusminski, C. M., Wang, Q. A., Hepler, C., Vishvanath, L., MacPherson, K. A., Spurgin, S. B., Sun, K., Holland, W. L. et al. (2016). Zfp423 maintains white adipocyte identity through suppression of the beige cell thermogenic gene program. *Cell Metab.* **23**, 1167-1184.

Slaats, G. G., Saldivar, J. C., Bacal, J., Zeman, M. K., Kile, A. C., Hynes, A. M., Srivastava, S., Nazmutdinova, J., den Ouden, K., Zagers, M. S. et al. (2015). DNA replication stress underlies renal phenotypes in CEP290-associated Joubert syndrome. *J. Clin. Invest.* **125**, 3657-3666.

Sleven, H., Welsh, S. J., Yu, J., Churchill, M. E. A., Wright, C. F., Henderson, A., Horvath, R., Rankin, J., Vogt, J., Magee, A. et al. (2017). De novo mutations in EBF3 cause a neurodevelopmental syndrome. *Am. J. Hum. Genet.* **100**, 138-150.

Tsai, R. Y. and Reed, R. R. (1997). Cloning and functional characterization of Roaz, a zinc finger protein that interacts with O/E-1 to regulate gene expression: implications for olfactory neuronal development. *J. Neurosci.* **17**, 4159-4169.

Tsai, R. Y. L. and Reed, R. R. (1998). Identification of DNA recognition sequences and protein interaction domains of the multiple-Zn-finger protein Roaz. *Mol. Cell. Biol.* **18**, 6447-6456.

Van Hooser, A., Goodrich, D. W., Allis, C. D., Brinkley, B. R. and Mancini, M. A. (1998). Histone H3 phosphorylation is required for the initiation, but not maintenance, of mammalian chromosome condensation. *J. Cell Sci.* **111**, 3497-3506.

Wallace, V. A. (1999). Purkinje-cell-derived Sonic hedgehog regulates granule neuron precursor cell proliferation in the developing mouse cerebellum. *Curr. Biol.* **9**, 445-448.

Wang, S. S., Tsai, R. Y. L. and Reed, R. R. (1997). The characterization of the Olf-1/EBF-like HLH transcription factor family: implications in olfactory gene regulation and neuronal development. *J. Neurosci.* **17**, 4149-4158.

Wang, B., Harrison, W., Overbeek, P. A. and Zheng, H. (2011). Transposon mutagenesis with coat color genotyping identifies an essential role for Skor2 in sonic hedgehog signaling and cerebellum development. *Development* **138**, 4487-4497.

Warming, S., Rachel, R. A., Jenkins, N. A. and Copeland, N. G. (2006). Zfp423 is required for normal cerebellar development. *Mol. Cell. Biol.* **26**, 6913-6922.

Wechsler-Reya, R. J. and Scott, M. P. (1999). Control of neuronal precursor proliferation in the cerebellum by Sonic Hedgehog. *Neuron* **22**, 103-114.

Weisheit, G., Gliem, M., Endl, E., Pfeffer, P. L., Busslinger, M. and Schilling, K. (2006). Postnatal development of the murine cerebellar cortex: formation and early dispersal of basket, stellate and Golgi neurons. *Eur. J. Neurosci.* **24**, 466-478.

Zhao, Y., Kwan, K.-M., Mailloux, C. M., Lee, W.-K., Grinberg, A., Wurst, W., Behringer, R. R. and Westphal, H. (2007). LIM-homeodomain proteins Lhx1 and Lhx5, and their cofactor Ldb1, control Purkinje cell differentiation in the developing cerebellum. *Proc. Natl. Acad. Sci. USA* **104**, 13182-13186.

Zhou, Y.-X., Zhao, M., Li, D., Shimazu, K., Sakata, K., Deng, C.-X. and Lu, B. (2003). Cerebellar deficits and hyperactivity in mice lacking Smad4. *J. Biol. Chem.* **278**, 42313-42320.

Zordan, P., Croci, L., Hawkes, R. and Consalez, G. G. (2008). Comparative analysis of proneural gene expression in the embryonic cerebellum. *Dev. Dyn.* **237**, 1726-1735.

SUPPLEMENTAL FIGURES

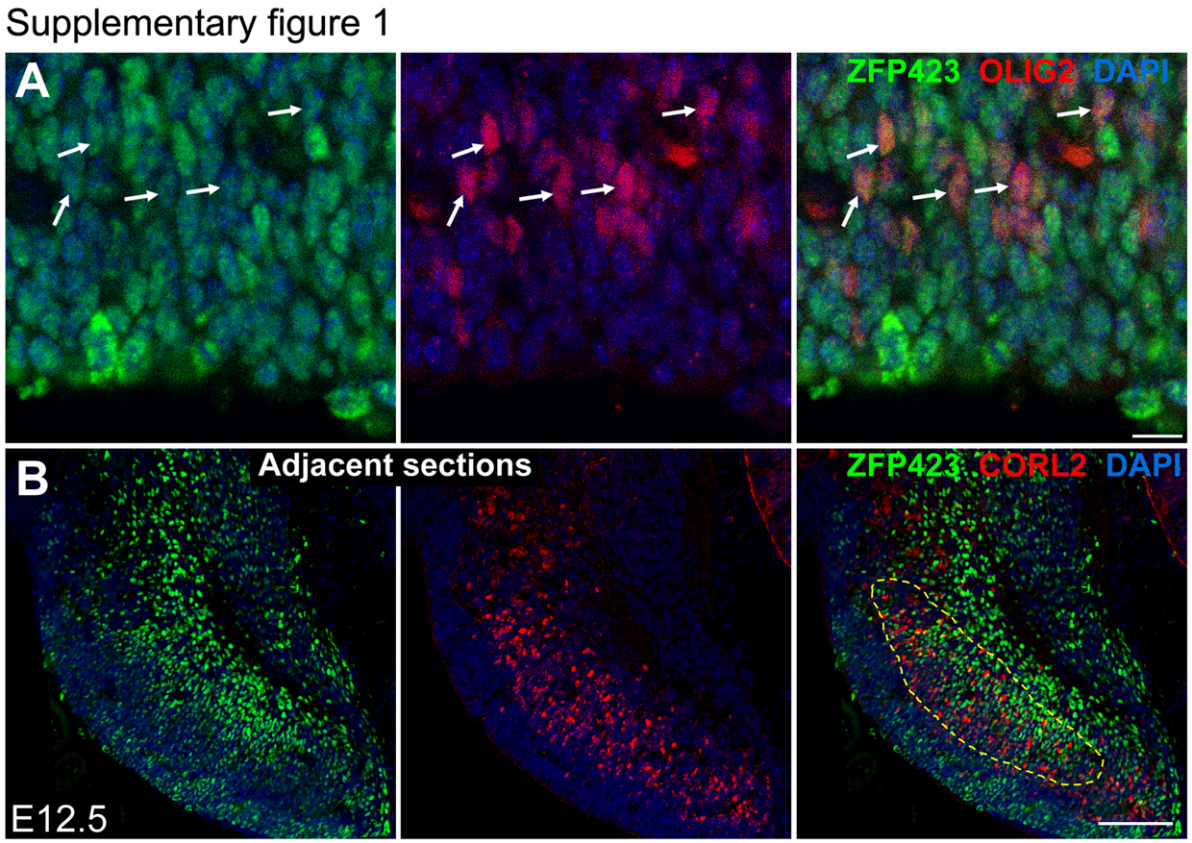

Fig. S1. ZFP423 expression overlaps partially with both OLIG2 and CORL2. Immunofluorescence staining of cerebellar sagittal sections at E12.5. ZFP423 is expressed in some OLIG2+ cells (**A**, arrows) and overlaps partially with CORL2+ domain (**B**). Size bars: **A**, 20µm; **B**, 100µm.

Supplementary figure 2

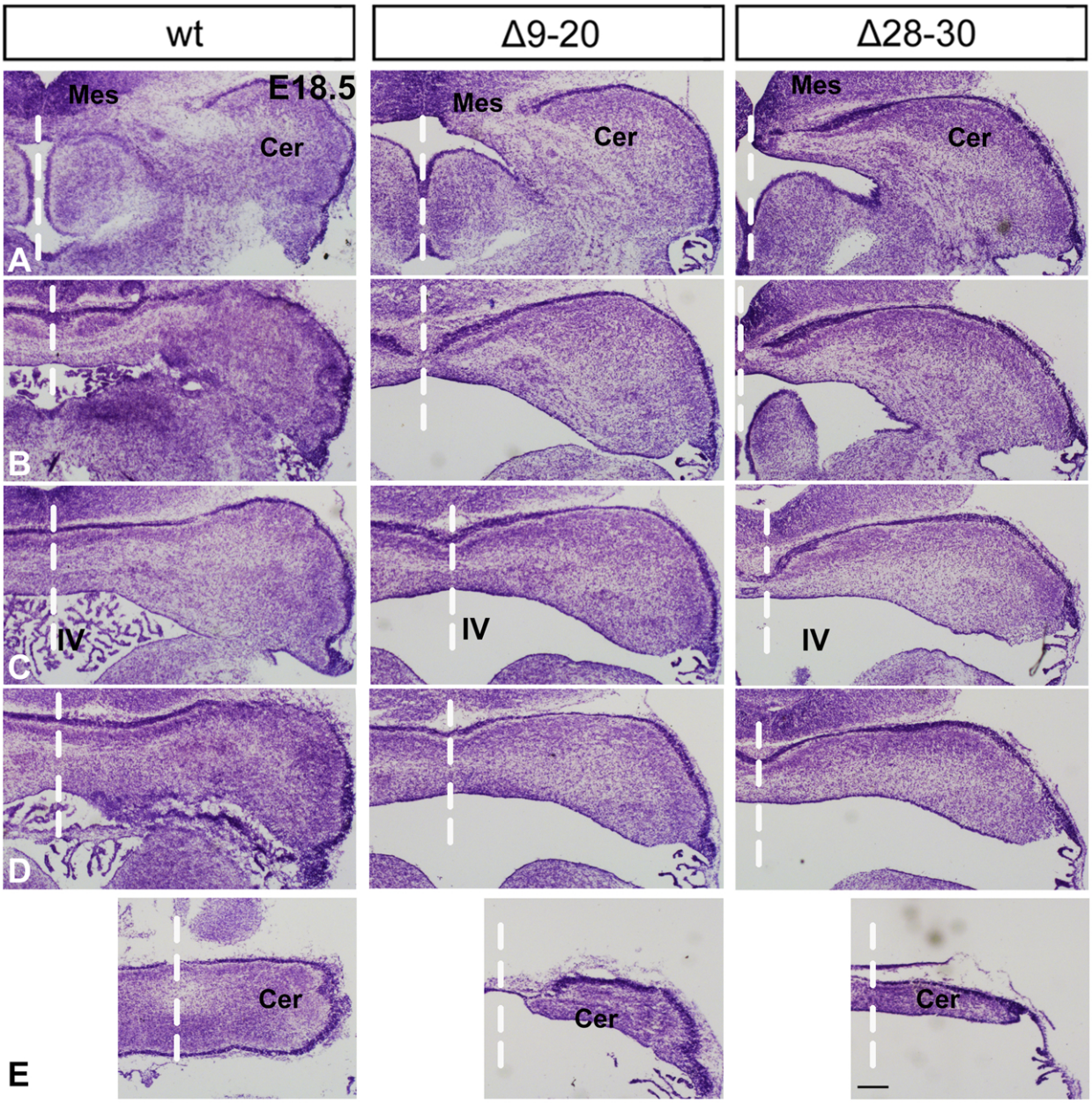

Fig. S2. Profound malformation in E18.5 mutant cerebella. Nissl staining of E18.5 embryo frontal sections showing a reconstructions of the main morphological differences between wt and mutants from rostral (**A**) to caudal (**E**). A severe cerebellar hypoplasia, with a markedly reduced vermis, is visible in both mutations. The Δ28-30 mutant features a more pronounced vermis deletion compare to the Δ9-20 (**C-D)**. Mes: mesencephalon; Cer: cerebellum; IV: fourth ventricle. Vertical dashed line represents the midline. Size Bar: 50µm.

Supplementary figure 3

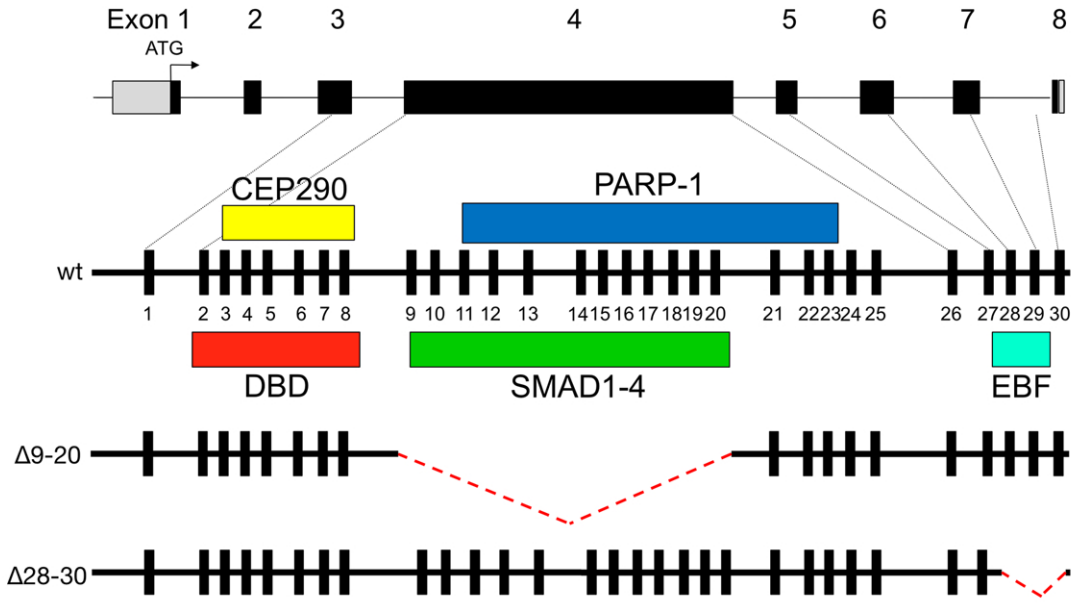

Fig. S3. ZFP423 is a nuclear scaffold establishing domain-specific interactions with multiple regulatory factors. ZFP423 / ZNF423 has been characterized as a nuclear scaffold protein mediating multiple protein-protein interactions. Briefly: CEP290 is a centrosomal protein implicated in centrosome and cilium development; PARP1 is a chromatin-modifying enzyme that triggers ADP-ribosylation of other nuclear proteins and has been implicated in DNA damage repair; SMAD proteins are nuclear transducers of BMP signaling; EBFs are transcription factors implicated in neuronal differentiation, migration and survival. See text for references.

Supplementary figure 4

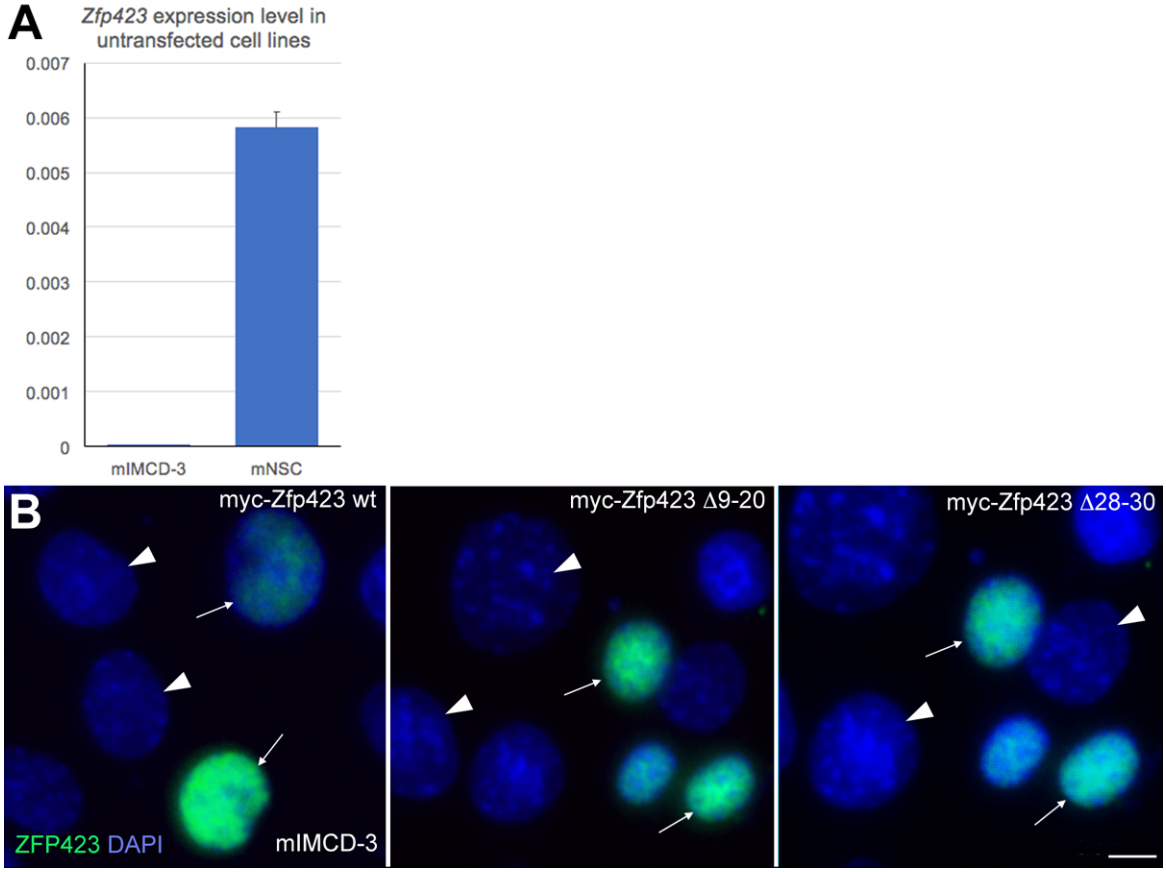

Fig. S4. Specific immunolabeling of ZFP423 by the sc-48785 antibody cells. A, RTqPCR indicates that *Zfp423* mRNA is undetectable in the IMCD-3 cell line. As a positive control, we used mouse cerebellar neural stem cells (NSCs) that strongly express *Zfp423*. **B,** IMCD-3 cell line transfected with tagged wt *Zfp423* and/or each of the mutant tagged constructs. Immunofluorescence for ZFP423 reveals that the Ab specifically recognizes transfected cells (arrows), while no signal is detectable in untrasfected cells (arrowheads). Size bar: 25µm.

Supplementary figure 5

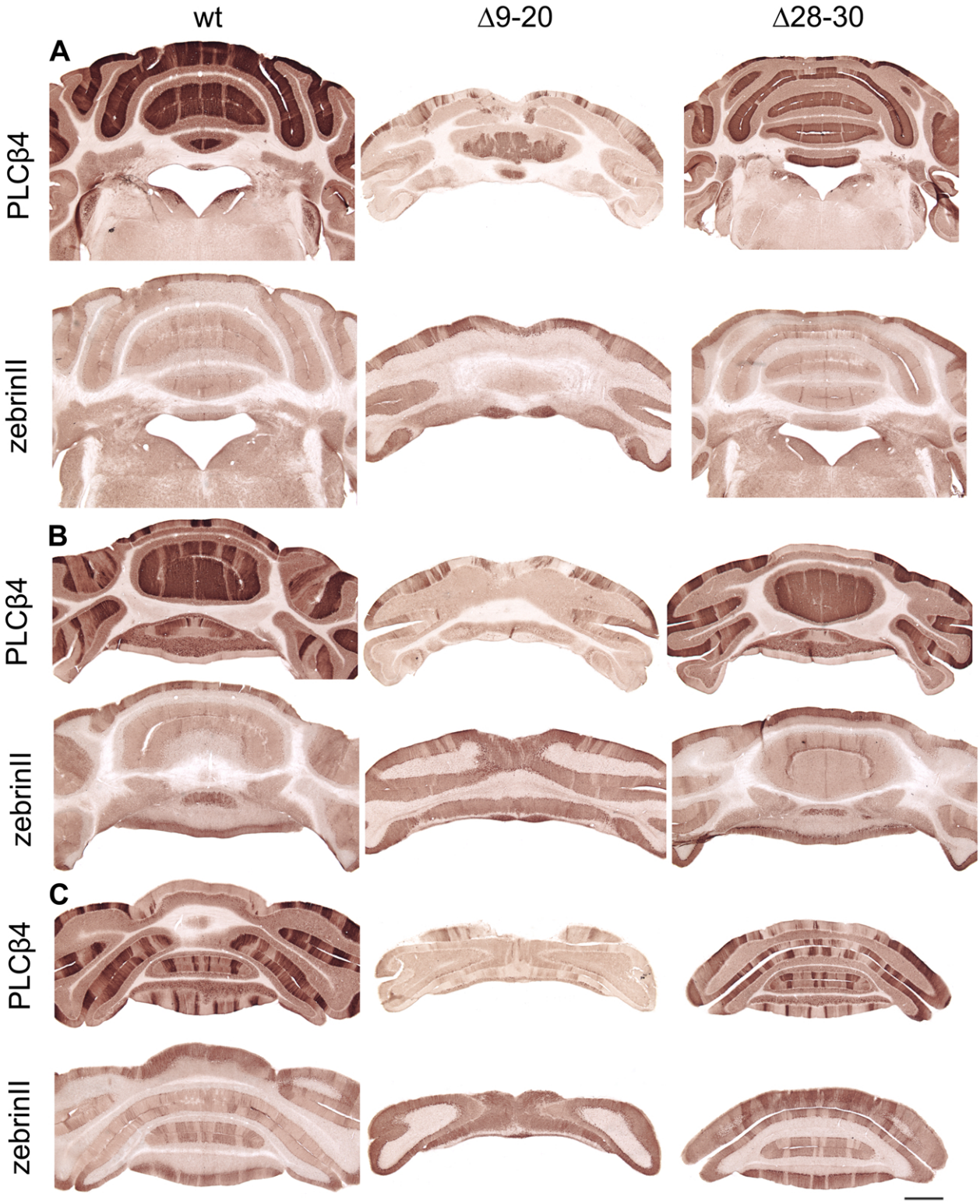

Fig. S5. ZebrinII-negative PCs are selectively lost in the Δ9-20 mutant. Zebrin II and PLCβ4 immunostaining of several P23 frontal cerebellar sections from rostral (**A**) to caudal (**C**). The results confirm a selective depletion of late-born PCs (mostly PLCβ4+) in Δ9-20 mutants, Throughout the cerebellum. Conversely, the Δ28-30 mutant cerebellum contains a balanced representation of early- (zebrin II+) and late-born (PLCβ4+) PCs and shows a dramatic decrease in size in the posterior area. Size bar: 1mm.

Supplementary figure 6

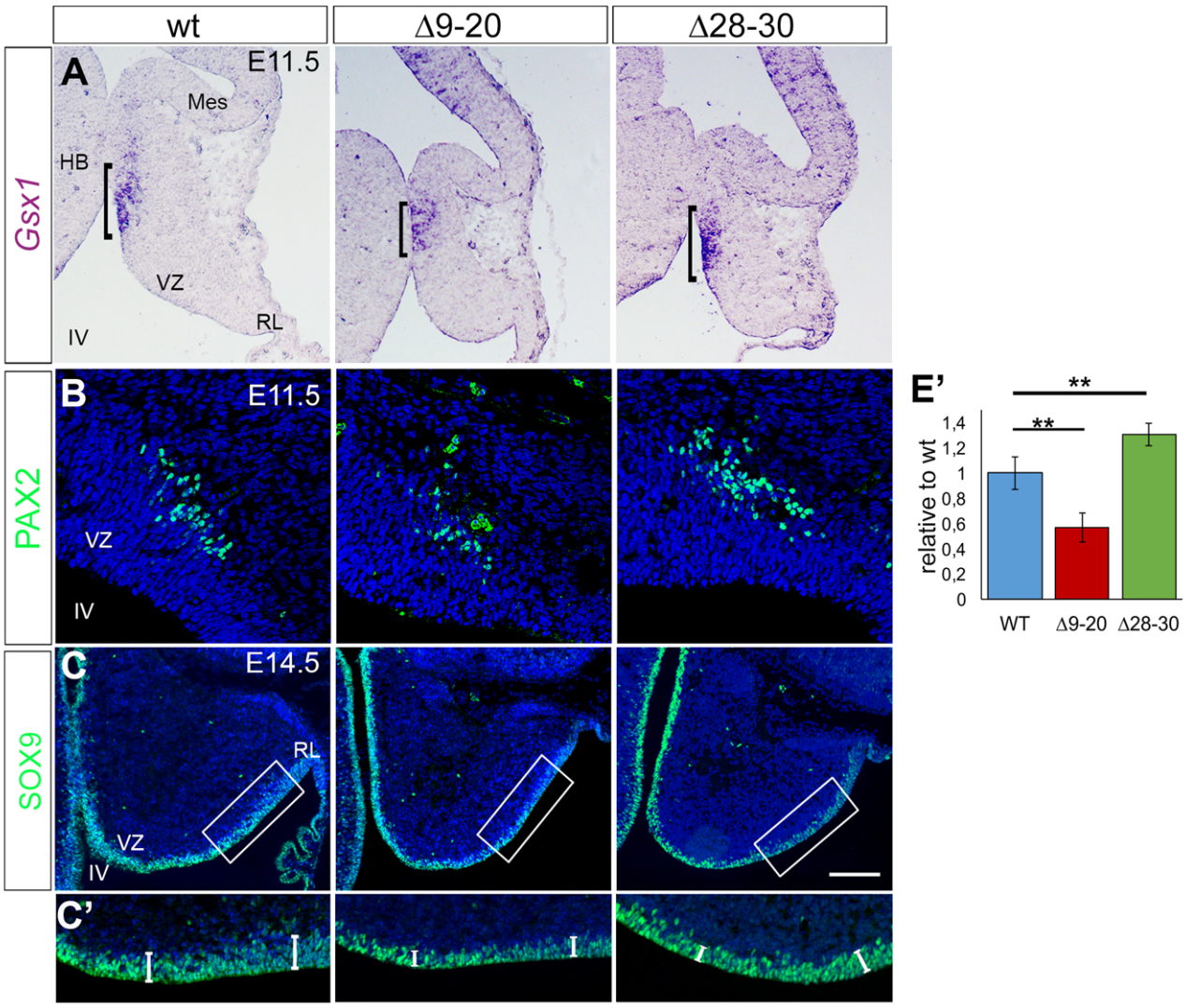

Fig. S6. Both GABA interneuron- and astrocyte progenitors are depleted in the Δ9-20 mutant. *In situ* hybridization (**A**) and immunofluorescence staining (**B**, **C**) of cerebellar sagittal sections at E11.5 (**A, B**) and E14.5 (**C**) (rostral to the left). **A**: the domain positive for *Gsx1* in the Δ9-20 primordium is reduced compared to the wt. **B:** PAX2-positive immunostaining of cerebellar sagittal sections at E11.5. The graph on the right shows that the number of PAX2+ cells decreases dramatically in the Δ9-20 mutant compared to the wt and increases in the Δ28-30 mutant (N=3/genotype; $^{**}p<0.001$, Fisher's exact test). **C:** SOX9-positive immunostaining of cerebellar sagittal sections at E14.5. **C'**: Magnification of the VZ (inset in **C**), showing an evident decrease in the number of SOX9+ cells in the Δ9-20 and Δ28-30 mutants, compared to the wt. The height of the white bars shows the different thickness of the SOX9+ domain, indicating a dramatic loss of SOX9 cells, particularly in the Δ9-20. Size bars: **A**: 150µm; **B**: 40µm; **C**: 200µm.

Supplementary figure 7

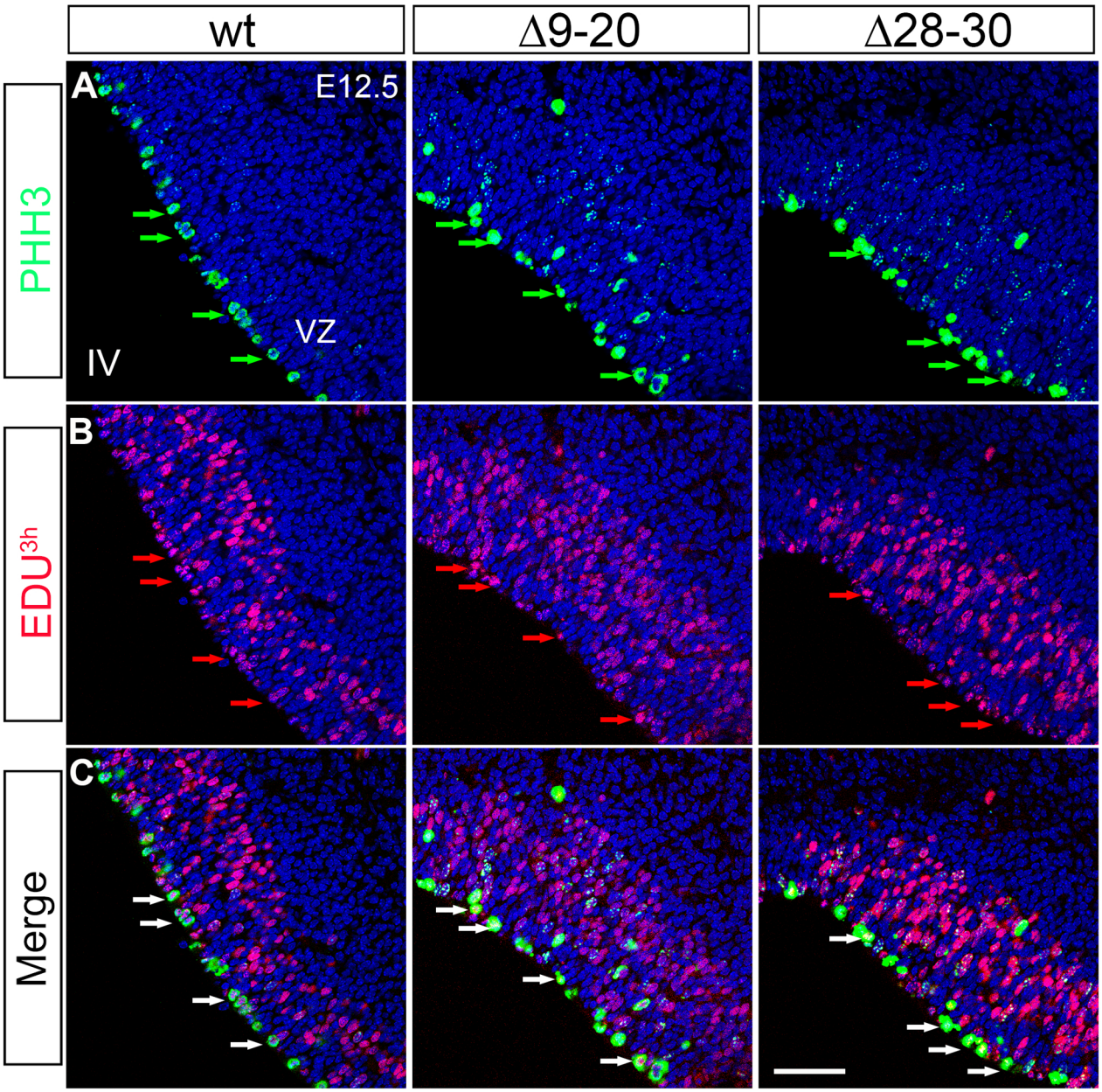

Fig. S7. In *Zfp423* mutants, fewer progenitors transit from S- to M-phase in 3 hours. A-C: Sagittal sections of the cerebellar primordium at E12.5 immunostained for PHH3 and EdU, single 3h pulse (rostral to the left). **A**: Full PHH3-positive cells are M-phase progenitors (green arrows). **B**: cells labeled by a single EdU 3h pulse (red) span the thickness of the VZ, including M-phase progenitors (red arrows). **C**: overlay of the 2 markers indicates that all M phase progenitors are also positive for EdU (white arrows) in the wt cerebellum and in both mutants. See text for discussion. Size bar: **A-C**: 40µm.